Computer Methods in Applied Mechanics and Engineering 445 (2025) 118149

Contents lists available at ScienceDirect

Comput. Methods Appl. Mech. Engrg.

journal homepage: www.elsevier.com/locate/cma

Locking mitigation in geometrically nonlinear solid beams through isogeometric analysis and a generalized constitutive approach

Leonardo Leonetti [a,b,1], Alessia Patton [c,*,1], Josef Kiendl [c]

[a] CIRTech Institute, HUTECH University, Ho Chi Minh City, Viet Nam
[b] Dipartimento di Ingegneria Informatica, Modellistica, Elettronica e Sistemistica, Università della Calabria, 87030, Rende (Cosenza), Italy
[c] Department of Civil Engineering and Environmental Sciences, University of the Bundeswehr Munich, Werner-Heisenberg-Weg 39, Neubiberg, 85579, Bayern, Germany

ARTICLE INFO

Keywords:
Solid beam
Isogeometric analysis
Locking mitigation techniques

ABSTRACT

This work proposes a novel geometrically nonlinear isogeometric solid-beam element, based on a one-dimensional interpolation of the displacement field. More specifically, the latter is approximated by a 12-parameter polynomial expansion in terms of displacement control variables and the cross-section parametric directions up to a bilinear term. To keep a beam-like modeling approach, the displacements are function of the beam's axis coordinate only through the control variables. This way, the model allows to flexibly capture the structure behavior with respect to e.g., bending and torsion, and a straightforward application of boundary conditions. The nature of the expansion is retained in the covariant axial and shear strains. Conversely, the transverse normal strains are kept constant and Poisson-thickness locking is treated by modifying the constitutive material matrix with exact integration within the beam's cross-section. This operation requires a proper representation of the strains that is carried out through the appropriate analytical expansion of the Jacobian without spurious terms. Additionally, by exploiting the concept of patch-wise reduced integration, namely employing cubic (C^2) isogeometric shape functions in an S_1^4 approximation space, shear and membrane locking are resolved with high efficiency, whereas the use of an isogeometric analysis framework naturally resolves curvature-thickness locking. The chosen expansion allows for a straightforward and efficient implementation given the possibility to construct the approximate strains *via* quadratic matrices and the performance of the proposed formulation is assessed by extensive numerical testing.

1. Introduction

Computer technology has refashioned our capacity to dissect solid structures belonging to mechanical systems into simplified elements. For instance, one-dimensional models, such as trusses and beams, can describe solid objects that are significantly larger in one dimension than the other two. This problem-reduction assumption, allowing for the abstraction of the beam's axis from the three-dimensional geometry, finds relevant application in engineering designs ranging from, civil, mechanical, energy, medical, and aerospace industries and typically entails increased computational efficiency and accuracy. For instance, structures such as flexible multibody systems, robots, and deployable large space structures can be conveniently modeled considering beams undergoing

* Corresponding author.
E-mail addresses: l.leonetti@hutech.edu.vn (L. Leonetti), alessia.patton@unibw.de (A. Patton), josef.kiendl@unibw.de (J. Kiendl).
[1] These authors contributed equally.

https://doi.org/10.1016/j.cma.2025.118149
Received 8 April 2025; Received in revised form 6 June 2025; Accepted 7 June 2025
Available online 7 July 2025
0045-7825/© 2025 The Authors. Published by Elsevier B.V. This is an open access article under the CC BY license (http://creativecommons.org/licenses/by/4.0/).

large rotations [1–3]. The concept of three-dimensional finite element (FE) modeling of geometrically exact beam theories has been originally developed in [4]. In this context, most of the research effort has been spent on the parametrization of three-dimensional finite rotations [5,6], given their non-vectorial character as well as non-commutative nature [4,7,8]. The difficulties of dealing with finite rotations pushed many authors towards alternative rotation-free discrete formulations [9–13]. In [14], beam-like structures based on the Reissner–Simo theory [7,15], undergoing the hypotheses of arbitrary large rotations and small strains have been efficiently solved. The ideas of objectivity and path independence are extensively examined in various works, including e.g., [16–21]. Due to the non-additivity characteristic of 3D rotations, the so-called path-dependent discretization strategies make the solution contingent upon the deformation history of the structure. Furthermore, the errors accumulated within the iterative solution process are never resolved, making the solution inaccurate even after only a few steps within the analysis. An alternative FE approach to model rotations including a significant rigid-body component are corotational (CR) formulations [22–24], allowing for the use of small strain models [25] superimposed to a rotating frame, such that nonlinearities due to large rotations can be successfully considered [23,26,27]. Earliest CR FE formulations keep the strain invariance under a rigid element motion ensuring path independence within a conservative problem [28] at the cost of non-symmetric and non-additive formulations, which penalize the efficiency and the ease of implementation. To overcome these challenges, recently [29] proposed the use of incremental nodal rotation vectors in a CR framework, making the model gain features which are favorable for nonlinear mechanical problems (i.e., rotational variables, objectivity, exact strain measure, path independence, and symmetric stiffness matrix for conservative loads) for any approximation.

Beam theories based on rotational degrees of freedom (dofs) complicate the coupling with solid elements and showcase challenges in achieving satisfactory robustness requirements. Also, advanced material modeling is not straightforward due to the stress state necessarily assumed within beam formulations. In contrast, the possibility of directly using three-dimensional constitutive laws in solid elements allows for a simplified simulation framework [30]. The concept of a solid-like structural model, entailing displacement dofs only, allows to overcome these drawbacks [31,32] and proves to be convenient especially when performing nonlinear analysis [2,33–35]. For the first time, this latter concept has been extended to beam structures in [36], and only recently, a few works have been published on this topic in the FE context [37,38]. However, displacement-based finite elements are intrinsically affected by locking, that can be resolved only if each static variable finds its kinematic counterpart in the analyzed energy expression [39]; otherwise this numerical pathology will lead to unreliable (overstiff) results. These numerical phenomena are exacerbated in beam structures formulated as solids, when modeled using one element within the cross-section. Among locking mitigation strategies, the Assumed Natural Strain (ANS) method is used in linear FE to typically alleviate curvature-thickness, as well as shear locking [32,36,38] by modifying the transverse shear and normal strain components and namely reducing the polynomial order of specific strain components. The so-called Poisson-thickness locking is caused, e.g., by the transverse contraction occurring under bending, which requires the transverse normal strains to be linear when the Poisson's ratio is non-zero. This latter type of locking can be treated by utilizing, e.g., the Enhanced Assumed Strain method (EAS) [36,40] first proposed in [41] and later extended to large displacements in [42]. The EAS method, conversely to the ANS technique, introduces an additional strain field as an incompatible mode to the conventional displacement-dependent compatible strains. Instead, the procedure proposed in [32], referred to as "generalized constitutive modeling", is a simple alternative to the EAS to remove Poisson-thickness locking *via* a modified constitutive law in terms of generalized stresses/strains, which assumes the transverse normal stress to be independent of the transverse coordinates. More in detail, the approach in [32] does not use additional variables, but instead assumes averaged values of the transverse normal strains, based on the simple kinematics considered for the sectional displacements. Combining different locking treatment techniques seems to be the key to generate very efficient numerical methods. For example, the nonlinear solid-shell element in [43] only uses three EAS parameters together with reduced integration [44]. The number of EAS parameters can be further reduced *via* the combined use of ANS, EAS, and reduced integration [45–47]. Mixed/hybrid formulations [48] have also been developed to efficiently resolve locking – namely, shear, curvature-thickness, and Poisson-thickness locking – effects [32,49,50] and, also, many authors [32,51] observe that mixed models perform better in path-following methods for geometrically nonlinear analyses. In this respect, a tentative explanation of this favorable behavior can be found in [52,53] and recently in [33], where it has been shown that FE methods with the same accuracy perform differently within a nonlinear solution process.

Introduced by Hughes et al. in 2005, Isogeometric Analysis (IGA) [54] is a higher-order numerical approach, alternative to the classical finite element method, designed to integrate geometric representations with numerical analysis. Additionally, owing to the high regularity of its basis functions, IGA exhibits improved accuracy per degree of freedom, an enhanced robustness with respect to standard finite elements, along with considerable versatility in accommodating various discretization approaches. Such developments facilitate more effective approaches to a variety of complex physical problems, spanning areas comprising solid mechanics, structural evaluation, and fluid dynamics. Particularly, we recall the successful simulation of e.g., Euler–Bernoulli beams [55–57], Timoshenko beams [58,59], Kirchhoff rods [60], Reissner–Mindlin [61,62] and Kirchhoff–Love shells [63–67]. In an IGA context, aside the ANS approach in [68], many attempts have been made to resolve locking effects in shell structures see, e.g., [69] and its extension to the nonlinear case [70], as well as the recent contributions in [71,72] to tackle membrane locking. Following the pioneering work of [58], in [2,66,73] it has been further demonstrated that an efficient way to alleviate shear and membrane locking is the use of selective and reduced numerical integration [74], where the notion of an approximation space of the target space is introduced to drive the choice of the most appropriate integration scheme. In this way, in [2,66] the locking is resolved by maintaining both the algebraic structure of the displacement-based models and the mixed format necessary for the efficient solution of the nonlinear problem. These favorable characteristics have been preserved by utilizing the MIP concept introduced in [75] and largely employed in [2,35,66] with the successful application to hyperelastic shells [73,76] and contact mechanics [77].

While extensive research has been carried out to treat locking in solid-shell IGA elements, to the best of our knowledge, only a limited number of studies addresses locking mitigation strategies for solid beams in an isogeometric framework. For instance, the solid-beam ANS element in [38] proposes a linear discretization within the structure's cross-section and leverages the EAS method to alleviate Poisson-thickness locking. Instead, the recent contribution in [78] does not require an EAS approach to modify the transverse normal strains, given the adopted quadratic IGA framework, which naturally alleviates Poisson-thickness, as well as curvature-thickness locking. The above considerations provide strong motivation for the development of strategies to tackle locking in solid-beam elements in an isogeometric context. Therefore, we propose a novel geometrically nonlinear isogeometric solid-beam element inspired by the techniques proposed in [2,33] for solid shells. Namely, in our extension the element is described by the sole displacement field, that is approximated by a 12-parameter polynomial expansion in terms of control variables and cross-section parametric directions up to a bilinear term. Instead, being the displacements a function only of the beam's axis coordinates though the control variables, we are able to provide a formulation that is closer to a beam-like modeling approach in comparison with the contributions in [38,78]. Notably, the new displacement variables have a similar interpretation to those used in beam models in the sense that the present formulation is able to describe, e.g., rotations, which are linearly mapped to the nodal displacements in a straightforward manner. This turns for instance into an easy implementation of boundary conditions. While the covariant axial and shear strains preserve a bilinear expansion structure, the transverse normal strains are maintained constant and Poisson-thickness locking is addressed by modifying the constitutive material matrix with exact integration within the beam's cross-section, following the strategy presented in [32]. Furthermore, we mitigate shear and membrane locking with high efficiency adopting a patch-wise reduced integration concept, which employs cubic (C^2) isogeometric shape functions in an S_1^4 approximation, whereas the use an isogeometric analysis framework allows to naturally resolve curvature-thickness locking [78].

The paper is structured as follows: Section 2 outlines the 12-parameter isogeometric solid-beam element's kinematics, the strain expansion, and details the analytical expansion of the Jacobian and its inverse without spurious terms to appropriately map the covariant strains into a local Cartesian framework to apply our Poisson-thickness locking mitigation strategy. The mapping can be carried out utilizing a closed-form matrix as detailed in Appendix A. Then, in Section 3, we focus on the solid-beam weak form and address the efficient discretization of the strain covariant components *via* quadratic matrices (see Appendix B). Section 4 outlines our complete locking mitigation strategy. The chosen quadrature rule, which uses cubic (C^2) isogeometric shape functions in an S_1^4 approximation space, allows for resolving membrane and shear locking. Furthermore, the use of an isogeometric analysis framework naturally eliminates curvature-thickness locking, whereas Poisson-thickness locking is treated here by providing a modified generalized constitutive matrix, that is analytically evaluated following a step-by-step procedure as detailed in Appendix C, and its partitioning can be straightforwardly utilized in the case of composites. The proposed approach considers an effective one-dimensional patch-wise reduced integration that results into a fast strategy for resolving linear and geometrically nonlinear problems, as showcased in Section 5. We finally draw our conclusions in Section 6.

2. The 12-parameter solid-beam model

In this section, we introduce our solid-beam model which can be conveniently detailed in terms of generalized strains by following a 1D description, as in the case of geometrically exact beam formulations. More specifically, we introduce the kinematics of the solid beam and describe the 12-parameter 1D-interpolation of the displacement field, that will be of aid to delineate the assumed polynomial expansion of the strain. Thus, we detail the appropriate mapping of this quantity, that is a key point in the implementation of the chosen Poisson-thickness locking removal strategy. In fact, we need to correctly identify the transverse normal strains which are defined in a local coordinate system aligned with the axis of the beam. This operation is naturally achieved utilizing a covariant basis, that also makes the nonlinear analysis more efficient, as strain measures and variations can be expressed using quadratic matrices. Then, the covariant basis is turned into a local Cartesian basis to properly account for the material. This choice also provides the flexibility to consider more complicated material behaviors (e.g., anisotropic materials) and geometries (such as skewed sections).

2.1. Kinematics

Therefore, the proposed model extends the work of [2] and can be used to straightforwardly simulate both isotropic and composite beams. Adopting a total Lagrangian formulation, the beam's axis is interpolated *via* a NURBS curve. Convective curvilinear coordinates $\boldsymbol{\xi} = [\xi^1, \xi^2, \xi^3]$, with $\xi^i \in [-1; 1]$ ($i = \{1, 2, 3\}$) are adopted, such that ξ^1 represents the axis coordinate, whereas $[\xi^2, \xi^3]$ identify the cross-section coordinates as detailed in Fig. 1. Each material point of the current configuration $\mathbf{x}(\xi^1, \xi^2, \xi^3)$ is described by its position vector $\mathbf{X}(\xi^1, \xi^2, \xi^3)$ in the reference configuration and the displacement field $\mathbf{u}(\xi^1, \xi^2, \xi^3)$ as

$$\mathbf{x}(\xi^1, \xi^2, \xi^3) = \mathbf{X}(\xi^1, \xi^2, \xi^3) + \mathbf{u}(\xi^1, \xi^2, \xi^3)\,. \tag{1}$$

Then, the covariant basis vectors in the undeformed and deformed configurations are obtained from the corresponding partial derivatives of the position vectors $\mathbf{X}$ and $\mathbf{x}$, respectively, as

$$\mathbf{G}_i = \mathbf{X}_{,i}\,, \qquad \mathbf{g}_i = \mathbf{x}_{,i} = \mathbf{G}_i + \mathbf{u}_{,i} \qquad \text{with} \quad i = \{1, 2, 3\}\,, \tag{2}$$

where $(.)_{,i}$ denotes the partial derivative with respect to the i-th component of the convective curvilinear coordinates $\boldsymbol{\xi}$, whereas the contravariant basis vectors in the undeformed configuration $\mathbf{G}^i$ can be retrieved from the dual basis property $\mathbf{G}_i \cdot \mathbf{G}^j = \delta_i^j$.

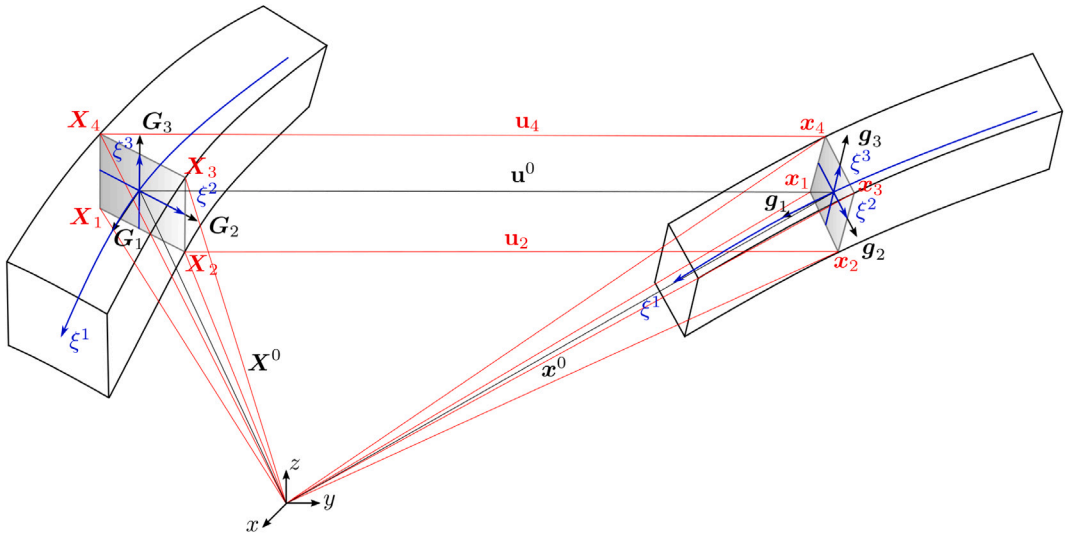

Fig. 1. 12-parameter solid-beam kinematics.

By assuming linear displacements in both the width and thickness directions of the beam's cross-section, the displacement field can be conveniently defined as a bilinear combination, along ξ^2 and ξ^3, of control variables, which depend on the solid-beam axis coordinate only (i.e., $\mathbf{u}_n = \mathbf{u}_n(\xi^1)$ with $n = \{1,2,3,4\}$), and the cross-section curvilinear convective coordinates $[\xi^2, \xi^3]$ as

$$\begin{aligned}\mathbf{u}(\xi^1,\xi^2,\xi^3) = &\frac{1}{2}(1-\xi^2)\frac{1}{2}(1-\xi^3)\mathbf{u}_1(\xi^1) + \frac{1}{2}(1+\xi^2)\frac{1}{2}(1-\xi^3)\mathbf{u}_2(\xi^1)\\ &+ \frac{1}{2}(1+\xi^2)\frac{1}{2}(1+\xi^3)\mathbf{u}_3(\xi^1) + \frac{1}{2}(1-\xi^2)\frac{1}{2}(1+\xi^3)\mathbf{u}_4(\xi^1),\end{aligned} \tag{3}$$

that can be straightforwardly reorganized as

$$\begin{aligned}\mathbf{u}(\xi^1,\xi^2,\xi^3) = &\underbrace{\frac{\mathbf{u}_1(\xi^1)+\mathbf{u}_2(\xi^1)+\mathbf{u}_3(\xi^1)+\mathbf{u}_4(\xi^1)}{4}}_{\mathbf{u}^0(\xi^1)} + \xi^2 \underbrace{\frac{\mathbf{u}_3(\xi^1)+\mathbf{u}_2(\xi^1)-\mathbf{u}_4(\xi^1)-\mathbf{u}_1(\xi^1)}{4}}_{\mathbf{u}^1(\xi^1)}\\ &+ \xi^3 \underbrace{\frac{\mathbf{u}_4(\xi^1)-\mathbf{u}_1(\xi^1)+\mathbf{u}_3(\xi^1)-\mathbf{u}_2(\xi^1)}{4}}_{\mathbf{u}^2(\xi^1)} + \xi^2\xi^3 \underbrace{\frac{\mathbf{u}_3(\xi^1)-\mathbf{u}_2(\xi^1)-\mathbf{u}_4(\xi^1)+\mathbf{u}_1(\xi^1)}{4}}_{\mathbf{u}^3(\xi^1)}.\end{aligned} \tag{4}$$

Then, the 1-D interpolation of the displacements as a function of ξ^1 (4) can be conveniently rewritten as

$$\mathbf{u}(\xi^1,\xi^2,\xi^3) = \mathbf{u}^0(\xi^1) + \xi^2\mathbf{u}^1(\xi^1) + \xi^3\mathbf{u}^2(\xi^1) + \xi^2\xi^3\mathbf{u}^3(\xi^1), \tag{5}$$

where the newly introduced symbols[2] $\mathbf{u}^k$ ($k = \{0,1,2,3\}$), in combination with ξ^2 and ξ^3 coordinates, highlight the nature of the chosen expansion. In fact, for a fixed coordinate along the beam's axis ξ^1, we underline in Eq. (5) the presence of a constant term, a linear quantity in ξ^2 and ξ^3, respectively, and a bilinear term in ξ^2, ξ^3, so to represent the translation of the barycenter of the solid-beam cross-section, its rotation about both cross-section axes, and torsion. In analogy to Eq. (5), the expansion to describe the beam's geometry in the reference configuration $\mathbf{X}$ can be defined *via* the coefficients $\mathbf{X}^k$ ($k = \{0,1,2,3\}$) up to a bilinear term in

[2] We highlight that it is simple to obtain the nodal displacements $\mathbf{u}_n$ from the expansion coefficients $\mathbf{u}^k$ ($k = \{0,1,2,3\}$) using the following relations:

$$\mathbf{u}_1 = \mathbf{u}^0 - \mathbf{u}^1 - \mathbf{u}^2 + \mathbf{u}^3, \quad \mathbf{u}_2 = \mathbf{u}^1 + \mathbf{u}^0 - \mathbf{u}^2 - \mathbf{u}^3,$$
$$\mathbf{u}_3 = \mathbf{u}^2 + \mathbf{u}^0 + \mathbf{u}^3 + \mathbf{u}^1, \quad \mathbf{u}_4 = \mathbf{u}^2 + \mathbf{u}^0 - \mathbf{u}^3 - \mathbf{u}^1.$$

ξ^2, ξ^3 as

$$\mathbf{X}(\xi^1, \xi^2, \xi^3) = \mathbf{X}^0(\xi^1) + \xi^2 \mathbf{X}^1(\xi^1) + \xi^3 \mathbf{X}^2(\xi^1) + \xi^2 \xi^3 \mathbf{X}^3(\xi^1) \,. \tag{6}$$

2.2. Strains

Hereinafter, Einstein's notation, i.e., repeated indices imply the summation of the involved components, is adopted unless otherwise stated. Thus, the Green–Lagrange strain tensor can be expressed as a subclass of the Seth-Hill strain measures[3] [79] as

$$\mathbf{E}^{(2)} = E_{ij}\, \mathbf{G}^i \otimes \mathbf{G}^j \,, \tag{7}$$

where E_{ij} are the covariant Green–Lagrange strain components in the undeformed configuration, which, once we define $(\cdot)$ as the scalar product, can be detailed as

$$E_{ij} = \frac{1}{2} \left(\mathbf{X}_{,i} \cdot \mathbf{u}_{,j} + \mathbf{u}_{,i} \cdot \mathbf{X}_{,j} + \mathbf{u}_{,i} \cdot \mathbf{u}_{,j} \right) \quad \text{with} \quad i, j = \{1, 2, 3\} \,. \tag{8}$$

For ease of readability, we focus herein on the description of the polynomial expansion for the linear strain components only, given the fact that their nonlinear counterpart follows the same expansion structure and can be obtained in a straightforward manner at the discrete level as detailed in Section 3.2 and Appendix A. Therefore, considering the suitable partial derivatives of Eqs. (5) and (6) within relation $\frac{1}{2} \left(\mathbf{X}_{,i} \cdot \mathbf{u}_{,j} + \mathbf{u}_{,i} \cdot \mathbf{X}_{,j} \right)$, the polynomial expansions of the linear strain measure components read

$$\begin{aligned}
E_{11} &= \underbrace{\mathbf{X}^{0\mathrm{T}}_{,1} \mathbf{u}^0_{,1}}_{E^0_{11}} + \xi^2 \underbrace{(\mathbf{X}^{0\mathrm{T}}_{,1} \mathbf{u}^1_{,1} + \mathbf{X}^{1\mathrm{T}}_{,1} \mathbf{u}^0_{,1})}_{E^1_{11}} + \xi^3 \underbrace{(\mathbf{X}^{0\mathrm{T}}_{,1} \mathbf{u}^2_{,1} + \mathbf{X}^{2\mathrm{T}}_{,1} \mathbf{u}^0_{,1})}_{E^2_{11}} \\
&\quad + \xi^2 \xi^3 \underbrace{(\mathbf{X}^{0\mathrm{T}}_{,1} \mathbf{u}^3_{,1} + \mathbf{X}^{3\mathrm{T}}_{,1} \mathbf{u}^0_{,1} + \mathbf{X}^{1\mathrm{T}}_{,1} \mathbf{u}^2_{,1} + \mathbf{X}^{2\mathrm{T}}_{,1} \mathbf{u}^1_{,1})}_{E^3_{11}} , \\
E_{22} &= \underbrace{\mathbf{X}^{1\mathrm{T}} \mathbf{u}^1}_{E^0_{22}} , \\
E_{33} &= \underbrace{\mathbf{X}^{2\mathrm{T}} \mathbf{u}^2}_{E^0_{33}} , \\
2E_{12} &= \underbrace{\mathbf{X}^{0\mathrm{T}}_{,1} \mathbf{u}^1 + \mathbf{X}^{1\mathrm{T}} \mathbf{u}^0_{,1}}_{E^0_{12}} + \xi^2 \underbrace{(\mathbf{X}^{1\mathrm{T}}_{,1} \mathbf{u}^1 + \mathbf{X}^{1\mathrm{T}} \mathbf{u}^1_{,1})}_{E^1_{12}} + \xi^3 \underbrace{(\mathbf{X}^{2\mathrm{T}}_{,1} \mathbf{u}^1 + \mathbf{X}^{0\mathrm{T}}_{,1} \mathbf{u}^3 + \mathbf{X}^{1\mathrm{T}} \mathbf{u}^2_{,1} + \mathbf{X}^{3\mathrm{T}} \mathbf{u}^0_{,1})}_{E^2_{12}} \\
&\quad + \xi^2 \xi^3 \underbrace{(\mathbf{X}^{1\mathrm{T}}_{,1} \mathbf{u}^3 + \mathbf{X}^{3\mathrm{T}}_{,1} \mathbf{u}^1 + \mathbf{X}^{1\mathrm{T}} \mathbf{u}^3_{,1} + \mathbf{X}^{3\mathrm{T}} \mathbf{u}^1_{,1})}_{E^3_{12}} , \\
2E_{13} &= \underbrace{\mathbf{X}^{0\mathrm{T}}_{,1} \mathbf{u}^2 + \mathbf{X}^{2\mathrm{T}} \mathbf{u}^0_{,1}}_{E^0_{13}} + \xi^2 \underbrace{(\mathbf{X}^{0\mathrm{T}}_{,1} \mathbf{u}^3 + \mathbf{X}^{1\mathrm{T}}_{,1} \mathbf{u}^2 + \mathbf{X}^{2\mathrm{T}} \mathbf{u}^1_{,1} + \mathbf{X}^{3\mathrm{T}} \mathbf{u}^0_{,1})}_{E^1_{13}} + \xi^3 \underbrace{(\mathbf{X}^{2\mathrm{T}}_{,1} \mathbf{u}^2 + \mathbf{X}^{2\mathrm{T}} \mathbf{u}^2_{,1})}_{E^2_{13}} \\
&\quad + \xi^2 \xi^3 \underbrace{(\mathbf{X}^{2\mathrm{T}}_{,1} \mathbf{u}^3 + \mathbf{X}^{3\mathrm{T}}_{,1} \mathbf{u}^2 + \mathbf{X}^{2\mathrm{T}} \mathbf{u}^3_{,1} + \mathbf{X}^{3\mathrm{T}} \mathbf{u}^2_{,1})}_{E^3_{13}} , \\
2E_{23} &= \underbrace{\mathbf{X}^{1\mathrm{T}} \mathbf{u}^2 + \mathbf{X}^{2\mathrm{T}} \mathbf{u}^1}_{E^0_{23}} + \xi^2 \underbrace{(\mathbf{X}^{1\mathrm{T}} \mathbf{u}^3 + \mathbf{X}^{3\mathrm{T}} \mathbf{u}^1)}_{E^1_{23}} + \xi^3 \underbrace{(\mathbf{X}^{3\mathrm{T}} \mathbf{u}^2 + \mathbf{X}^{2\mathrm{T}} \mathbf{u}^3)}_{E^2_{23}} + \xi^2 \xi^3 \underbrace{(\mathbf{X}^{3\mathrm{T}} \mathbf{u}^3 + \mathbf{X}^{3\mathrm{T}} \mathbf{u}^3)}_{E^3_{23}} ,
\end{aligned} \tag{9}$$

where, for the axial strain E_{11}, the transverse shears E_{12}, E_{13}, and shear component E_{23}, we retain only the terms bilinear in the cross-section coordinates ξ^2, ξ^3 to capture bending, torsion, and combined behaviors. Conversely, the transverse normal strains E_{22}, E_{33} are kept coherently constant as we will resolve Poisson-thickness locking by modifying the constitutive material matrix. Then, by assuming the transverse normal stresses being independent of the thickness parameter directions ξ^2 and ξ^3 (as detailed in Section 4.1), the transverse normal strains can only represent the cross-section average value [32].

[3] Strain tensors belonging to the Seth-Hill strain measure class are denoted with superscript $(.)^{(m)}$ as $\mathbf{E}^{(m)} = \frac{1}{m}(\mathbf{U} - \mathbf{I})$, being $m \in \mathbb{N}^*$, and $\mathbf{U}$ and $\mathbf{I}$ the right stretch and the identity tensor, respectively.

Thus, the non-zero covariant strains in Eq. (9) are collected in the vector

$$\mathbf{E}=\begin{bmatrix}E_{11}\\E_{22}\\E_{33}\\E_{12}\\E_{23}\\E_{13}\end{bmatrix}=\begin{bmatrix}E^0_{11}+\xi^2E^1_{11}+\xi^3E^2_{11}+\xi^2\xi^3E^3_{11}\\E^0_{22}\\E^0_{33}\\E^0_{12}+\xi^2E^1_{12}+\xi^3E^2_{12}+\xi^2\xi^3E^3_{12}\\E^0_{23}+\xi^2E^1_{23}+\xi^3E^2_{23}+\xi^2\xi^3E^3_{23}\\E^0_{13}+\xi^2E^1_{13}+\xi^3E^2_{13}+\xi^2\xi^3E^3_{13}\end{bmatrix}, \tag{10}$$

where we highlight the constant, linear, and bilinear terms in the strain expansion. Then, the strain vector can be conveniently further partitioned into sub-blocks as

$$\mathbf{E}^0_t=\begin{bmatrix}E^0_{22}\\E^0_{33}\end{bmatrix},\quad \mathbf{E}^k_s=\begin{bmatrix}2E^k_{12}\\2E^k_{23}\\2E^k_{13}\end{bmatrix}\quad\text{with}\quad k=\{0,1,2,3\}, \tag{11}$$

emphasizing the transverse normal $\mathbf{E}^0_t$ and shear strains $\mathbf{E}^i_s$, respectively.

2.3. Map of the strain into local Cartesian coordinates

To address the issue of Poisson-thickness locking, we will modify the material properties of the beam, requiring the strain to be represented within a local Cartesian coordinate system. Therefore, it is of paramount importance to obtain a coherent representation of the local Cartesian strains without spurious extra terms. This operation is achieved by mapping the covariant strain (7) through $\bar{\mathbf{E}}^{(2)}=\mathbf{J}^{-1}\mathbf{E}^{(2)}\mathbf{J}^{-\mathrm{T}}$, such that, with $\mathbf{J}$ and $\mathbf{J}^{-1}$, we denote the Jacobian and its inverse, respectively. The latter relation can be further detailed in Voigt's notation as $\bar{\mathbf{E}}=\mathbf{T}\mathbf{E}$, where $\mathbf{T}$ matrix is function of $\mathbf{J}$ and $\mathbf{J}^{-1}$, which consider a polynomial expansion up to a bilinear term in ξ^2 and ξ^3 coordinates and are defined as:

$$\mathbf{J}(\xi^1,\xi^2,\xi^3)=\mathbf{J}_0(\xi^1)+\xi^2\mathbf{J}_1(\xi^1)+\xi^3\mathbf{J}_2(\xi^1)+\xi^2\xi^3\mathbf{J}_3(\xi^1), \tag{12}$$

$$\mathbf{J}^{-1}(\xi^1,\xi^2,\xi^3)=\mathbf{J}_0^{-1}(\xi^1)+\xi^2\mathbf{J}_1^{-1}(\xi^1)+\xi^3\mathbf{J}_2^{-1}(\xi^1)+\xi^2\xi^3\mathbf{J}_3^{-1}(\xi^1). \tag{13}$$

In Eqs. (12) and (13), the Jacobian expansion matrices of coefficients are detailed as

$$\mathbf{J}_0(\xi^1)=\begin{bmatrix}\mathbf{X}^0_{,1} & \mathbf{X}^1 & \mathbf{X}^2\end{bmatrix},\quad \mathbf{J}_1(\xi^1)=\begin{bmatrix}\mathbf{X}^1_{,1} & \mathbf{0} & \mathbf{X}^3\end{bmatrix}, \tag{14}$$

$$\mathbf{J}_2(\xi^1)=\begin{bmatrix}\mathbf{X}^2_{,1} & \mathbf{X}^3 & \mathbf{0}\end{bmatrix},\quad \mathbf{J}_3(\xi^1)=\begin{bmatrix}\mathbf{X}^3_{,1} & \mathbf{0} & \mathbf{0}\end{bmatrix}, \tag{15}$$

whereas the inverse Jacobian ones (namely $\mathbf{J}_k^{-1}(\xi^1)$, with $k=\{0,1,..3\}$) are derived in Appendix B following the identity matrix theorem. Coherently, also the transformation matrix $\mathbf{T}$ follows the same expansion

$$\mathbf{T}=\mathbf{T}^0+\xi^2\mathbf{T}^1+\xi^3\mathbf{T}^2+\xi^2\xi^3\mathbf{T}^3, \tag{16}$$

such that its coefficients read

$$\mathbf{T}^k=\begin{bmatrix}T^k_{1111} & T^k_{1122} & T^k_{1133} & T^k_{1112} & T^k_{1123} & T^k_{1113}\\T^k_{2211} & T^k_{2222} & T^k_{2233} & T^k_{2212} & T^k_{2223} & T^k_{2213}\\T^k_{3311} & T^k_{3322} & T^k_{3333} & T^k_{3312} & T^k_{3323} & T^k_{3313}\\T^i_{1211} & T^k_{1222} & T^k_{1233} & T^k_{1212} & T^k_{1223} & T^k_{1213}\\T^k_{2311} & T^k_{2322} & T^k_{2333} & T^k_{2312} & T^k_{2323} & T^k_{2313}\\T^k_{1311} & T^k_{1322} & T^k_{1333} & T^k_{1312} & T^k_{1323} & T^k_{1313}\end{bmatrix}. \tag{17}$$

A detailed derivation of the coefficients $\mathbf{T}^k$ (with $k=\{0,1,\dots,3\}$) can be found in Appendix A.

3. Solid-beam weak form and discretization

In this section, we introduce the second Piola–Kirchhoff stress tensor and derive its contravariant resultants, dual to the covariant strain tensor. This operation is carried out invoking the invariance of the internal work that gives raise to the weak form of our model. Then, we proceed to detail the discretization of the covariant strain to approximate the weak form, in a very straightforward manner *via* quadratic matrices, by directly providing their closed-form expressions.

3.1. Weak form

The stress is described by using the second Piola–Kirchhoff stress tensor

$$\mathbf{S}^{(2)}=S^{ij}\,\mathbf{G}_i\otimes\mathbf{G}_j \tag{18}$$

and the material is assumed to be linear elastic

$$\mathbf{S}^{(2)} = \mathbb{C} : \mathbf{E}^{(2)}, \quad \mathbf{E}^{(2)} = \mathbb{S} : \mathbf{S}^{(2)}, \tag{19}$$

where $(:)$ means double scalar product, while $\mathbb{C} = \mathbb{C}^{ijhk}\mathbf{G}_i \otimes \mathbf{G}_j \otimes \mathbf{G}_h \otimes \mathbf{G}_k$ and $\mathbb{C}^{-1} = \mathbb{S} = \mathbb{S}_{ijhk}\mathbf{G}^i \otimes \mathbf{G}^j \otimes \mathbf{G}^h \otimes \mathbf{G}^k$ are the stiffness and compliance elastic IV-order tensors, respectively. Therefore, the introduced stress and strain components read

$$S^{ij} = \mathbb{C}^{ijhk}E_{hk}, \quad E_{ij} = \mathbb{S}_{ijhk}S^{hk}, \tag{20}$$

and, by collecting the contravariant stress components in Voigt's notation $\mathbf{S} = [S^{11}, S^{22}, S^{33}, S^{12}, S^{23}, S^{13}]^{\mathrm{T}}$, we can partition $\mathbf{S}$ into the following sub-blocks

$$\mathbf{S}_t = \begin{bmatrix} S^{22} \\ S^{33} \end{bmatrix}, \quad \mathbf{S}_s = \begin{bmatrix} S^{12} \\ S^{23} \\ S^{13} \end{bmatrix}, \tag{21}$$

that highlight the transverse normal $\mathbf{S}_t$ and shear stresses $\mathbf{S}_s$, respectively. The generalized contravariant stress resultants, once the kinematic model is assumed, are automatically given as work conjugate variables to $\mathbf{E}$, by ensuring the invariance of the internal work

$$\mathcal{W} = \int_V \mathbf{S}^{\mathrm{T}}\mathbf{E}\mathrm{d}V = \int_\ell \left(\sum_{k=0}^{3} \mathcal{N}^k E_{11}^k + \boldsymbol{\mathcal{S}}_t^{0\mathrm{T}}\mathbf{E}_t^0 + \sum_{k=0}^{3} \boldsymbol{\mathcal{T}}^{k\mathrm{T}}\mathbf{E}_s^k \right) \mathrm{d}\ell, \tag{22}$$

where $\int_\ell (\ldots)\,\mathrm{d}\ell = 4\int_{\xi_i^1}^{\xi_{i+1}^1} (\ldots)\det(\mathbf{J}(\xi^1, 0, 0))\mathrm{d}\xi^1$ and $\mathbf{J}$ denotes the Jacobian matrix (12). Thus, the relevant generalized contravariant stress resultants can be retrieved from (22) following the strain counterpart bilinear polynomial expansion for the axial strain E_{11}

$$\begin{aligned} &\mathcal{N}^0 = \frac{1}{4}\int_{-1}^{1}\int_{-1}^{1} S^{11}\mathrm{d}\xi^2\mathrm{d}\xi^3, \qquad \mathcal{N}^1 = \frac{1}{4}\int_{-1}^{1}\int_{-1}^{1} \xi^2 S^{11}\mathrm{d}\xi^2\mathrm{d}\xi^3, \quad \mathcal{N}^2 = \frac{1}{4}\int_{-1}^{1}\int_{-1}^{1} \xi^3 S^{11}\mathrm{d}\xi^2\mathrm{d}\xi^3, \\ &\mathcal{N}^3 = \frac{1}{4}\int_{-1}^{1}\int_{-1}^{1} \xi^2\xi^3 S^{11}\mathrm{d}\xi^2\mathrm{d}\xi^3, \quad \boldsymbol{\mathcal{S}}_t^0 = \frac{1}{4}\int_{-1}^{1}\int_{-1}^{1} \mathbf{S}_t\mathrm{d}\xi^2\mathrm{d}\xi^3, \end{aligned} \tag{23}$$

as well as the transverse and shear strain components E_{12}, E_{13}, and E_{23}

$$\begin{aligned} &\boldsymbol{\mathcal{T}}^0 = \frac{1}{4}\int_{-1}^{1}\int_{-1}^{1} \mathbf{S}_s\mathrm{d}\xi^2\mathrm{d}\xi^3, \qquad \boldsymbol{\mathcal{T}}^1 = \frac{1}{4}\int_{-1}^{1}\int_{-1}^{1} \xi^2\mathbf{S}_s\mathrm{d}\xi^2\mathrm{d}\xi^3, \\ &\boldsymbol{\mathcal{T}}^2 = \frac{1}{4}\int_{-1}^{1}\int_{-1}^{1} \xi^3\mathbf{S}_s\mathrm{d}\xi^2\mathrm{d}\xi^3, \quad \boldsymbol{\mathcal{T}}^3 = \frac{1}{4}\int_{-1}^{1}\int_{-1}^{1} \xi^2\xi^3\mathbf{S}_s\mathrm{d}\xi^2\mathrm{d}\xi^3. \end{aligned} \tag{24}$$

In Eq. (22), $\mathbf{E}_t^0$ is the covariant transverse normal strain vector that is work-conjugate to $\mathbf{S}_t$ and its suitable modified definition to treat Poisson-thickness locking, as well as geometrical meaning, will be discussed in detailed in Section 4.

3.2. Discretized element covariant strain components: compact expressions via quadratic matrices

In Section 2.2, we only detailed the polynomial expansion of the linear part of Eq. (8), namely, $\frac{1}{2}\left(\mathbf{X}_{,i}\cdot\mathbf{u}_{,j} + \mathbf{u}_{,i}\cdot\mathbf{X}_{,j}\right)$. However, in the following we will describe the nonlinear counterpart of the expansion, as it follows the same structure of the linear contribution and can be obtained in a straightforward manner focusing on the discrete level. In fact, if we recall the covariant strain component definition, we can additively decompose the strain in a linear E_{ij}^L and nonlinear part E_{ij}^{NL}

$$E_{ij} = \left[\frac{1}{2}\left(\mathbf{X}_{,i}\cdot\mathbf{u}_{,j} + \mathbf{u}_{,i}\cdot\mathbf{X}_{,j}\right)\right] + \left[\frac{1}{2}\left(\mathbf{u}_{,i}\cdot\mathbf{u}_{,j}\right)\right] = E_{ij}^{\mathrm{L}}(\boldsymbol{\xi}, \mathbf{X}, \mathbf{u}) + \frac{1}{2}E_{ij}^{\mathrm{NL}}(\boldsymbol{\xi}, \mathbf{u}, \mathbf{u}),$$

where we highlight the dependence of the strain on the geometry and the displacement field.

Following the isoparametric paradigm and focusing on the element discretization, the geometry and displacement field are classically interpolated as

$$\mathbf{X}_e = \mathbf{N}^e\hat{\mathbf{X}}_e, \quad \mathbf{u}_e = \mathbf{N}^e\hat{\mathbf{d}}_e, \tag{25}$$

where we have collected the nodal components in the vectors $\mathbf{X}_e = \left[\left(\mathbf{X}^0\right)^{\mathrm{T}}, \left(\mathbf{X}^1\right)^{\mathrm{T}}, \left(\mathbf{X}^2\right)^{\mathrm{T}}, \left(\mathbf{X}^3\right)^{\mathrm{T}}\right]^{\mathrm{T}}$ and $\mathbf{d}_e = \left[\left(\mathbf{u}^0\right)^{\mathrm{T}}, \left(\mathbf{u}^1\right)^{\mathrm{T}}, \left(\mathbf{u}^2\right)^{\mathrm{T}}, \left(\mathbf{u}^3\right)^{\mathrm{T}}\right]^{\mathrm{T}}$, respectively, whereas with $\mathbf{N}_e$ we denote the element isogeometric shape function matrix. Then, substituting the element approximations (25) into the polynomial expansion (9) of the Green–Lagrange covariant strain components in Voigt's notation and repeating the operation for the nonlinear part of the strain, that carries the tensor structure as for its linear counterpart, we obtain the sum of two quadratic forms, namely

$$E_{ij}^e = \left(\mathbf{X}_e^{\mathrm{T}}\mathbf{Q}_{ij}(\boldsymbol{\xi}) + \frac{1}{2}\mathbf{d}_e^{\mathrm{T}}\mathbf{Q}_{ij}(\boldsymbol{\xi})\right)\mathbf{d}_e, \tag{26}$$

where the symmetric matrix $\mathbf{Q}_{ij}$ associated to the quadratic form naturally showcases the same polynomial expansion up to a bilinear term in ξ^2, ξ^3

$$\mathbf{Q}_{ij} = \mathbf{Q}_{ij}^0 + \xi^2\mathbf{Q}_{ij}^1 + \xi^2\mathbf{Q}_{ij}^2 + \xi^2\xi^3\mathbf{Q}_{ij}^3, \tag{27}$$

for which closed-form expression of $\mathbf{Q}_{ij}^{k}$ coefficients (with $k = \{0, 1, \dots, 3\}$) can be found in Appendix B.

4. Combined isogeometric locking-mitigation strategy *via* modified constitutive behavior and high-order patch-wise reduced integration

In this section, we detail our locking mitigation strategy that exploits the combined use of a modified constitutive behavior to treat Poisson-thickness locking, whereas shear and membrane locking are tackled *via* patch-wise reduced integration. Furthermore, the adopted isogeometric framework naturally eases curvature-thickness locking, profiting from the high-order continuity properties of the IGA shape functions and their superior geometrical modeling capabilities [78].

4.1. Strain modification via constitutive modeling and stress resultants

Adopting $\bar{E}_{22}$ and $\bar{E}_{33}$ constant along the cross-section coordinate directions, leads to the so-called Poisson-thickness locking. This numerical pathology is caused by the coupling of the axial strain, *via* a non-zero Poisson's ratio, with the transverse normal strains that need to be at least linear. A classical remedy is the EAS method [36], such that Poisson-thickness locking is cured by a linear enrichment of the transverse normal strains, which resolves also drawbacks when the material behavior approaches the incompressible limit (i.e., $\nu = 0.5$). In [32], the authors discuss, for homogeneous materials, the enforcement of plane stress conditions [80] as a possible locking-remedy for thin structures. Adopting instead a hybrid-stress formulation, Poisson-thickness locking is resolved by assuming the transverse normal stress $\bar{S}^{22}$ and $\bar{S}^{33}$ to be independent of the transverse coordinates (namely, ξ^2 and ξ^3) [36,49]. The strategy in [32] proposes a modified constitutive approach that turns out to resolve several inconsistent predictions associated with the EAS method and plane stress enforcement and represents a simple and effective way to remove Poisson-thickness locking, tested in the solid-shell case. Thus, in this work we propose its generalization to solid beams. Hereinafter, we highlight that the considered strains, relevant in the discussion of the locking strategy, are mapped in a local Cartesian reference system (see Section 2.3). By leveraging on the hybrid-stress approach and generalizing the concept used for the solid-shell model in [32,81], the element transverse normal stresses $\bar{S}^{22}$ and $\bar{S}^{33}$ are here taken to be independent of ξ^2 and ξ^3. This allows for an analytical pre-integration of the generalized constitutive matrix, which is particularly effective also in the analysis of composites. To this aim, the material constitutive behavior (anisotropic), expressed in matrix form in the chosen local Cartesian element reference system except for blocks corresponding to the shear components $2\bar{E}_{12}$, $2\bar{E}_{13}$, and $2\bar{E}_{23}$, is partitioned as

$$\begin{bmatrix} \bar{E}_{11} \\ \bar{\mathbf{E}}_t \end{bmatrix} = \begin{bmatrix} \bar{\mathbb{S}}_{1111} & \bar{\mathbb{S}}_{mt} \\ \bar{\mathbb{S}}_{mt}^{\mathrm{T}} & \bar{\mathbb{S}}_{tt} \end{bmatrix} \begin{bmatrix} \bar{S}^{11} \\ \bar{\mathbf{S}}_t \end{bmatrix}, \tag{28}$$

where

$$\bar{\mathbb{S}}_{mt} = \begin{bmatrix} \bar{\mathbb{S}}_{1122} & \bar{\mathbb{S}}_{1133} \end{bmatrix}, \quad \bar{\mathbb{S}}_{tt} = \begin{bmatrix} \bar{\mathbb{S}}_{2222} & \bar{\mathbb{S}}_{2233} \\ \bar{\mathbb{S}}_{3322} & \bar{\mathbb{S}}_{3333} \end{bmatrix}, \tag{29}$$

whereas the shear blocks of the constitutive matrix are treated conventionally. The system of Eqs. (28) is solved for $\bar{S}^{11}$ and $\bar{\mathbf{E}}_t$

$$\bar{S}^{11} = \frac{1}{\bar{\mathbb{S}}_{1111}} \bar{E}_{11} - \frac{\bar{\mathbb{S}}_{mt}}{\bar{\mathbb{S}}_{1111}} \bar{\mathbf{S}}_t = A\bar{E}_{11} + \mathbf{B}\bar{\mathbf{S}}_t, \tag{30}$$

$$\bar{\mathbf{E}}_t = -\mathbf{B}^{\mathrm{T}} \bar{E}_{11} + \mathbf{D}\bar{\mathbf{S}}_t, \tag{31}$$

where

$$A = \frac{1}{\bar{\mathbb{S}}_{1111}}, \quad \mathbf{B} = -A\bar{\mathbb{S}}_{mt}, \quad \mathbf{D} = \bar{\mathbb{S}}_{tt} + \bar{\mathbb{S}}_{mt}^{\mathrm{T}} \mathbf{B}. \tag{32}$$

By assuming $\bar{S}^{22}$ and $\bar{S}^{33}$ to be independent of ξ^2 and ξ^3, the average transverse normal strains are evaluated as

$$\bar{\mathbf{E}}_t^0 = \frac{1}{4} \int_{-1}^{1} \int_{-1}^{1} \bar{\mathbf{E}}_t \mathrm{d}\xi^2 \mathrm{d}\xi^3 = \frac{1}{4} \int_{-1}^{1} \int_{-1}^{1} \left(-\mathbf{B}^{\mathrm{T}} \bar{E}_{11} + \mathbf{D}\bar{\mathbf{S}}_t \right) \mathrm{d}\xi^2 \mathrm{d}\xi^3. \tag{33}$$

In this way, the compatibility relations (10) corresponding to the transverse normal strains are from now on geometrically referred to the cross-section average values (33). Furthermore, the proposed approach not only resolves Poisson-thickness locking, as it will be showcased in the numerical section, but makes the model particularly efficient given the fact that no additional integration points need to be positioned within the solid-beam section. By using the expansion chosen for $\bar{E}_{11}$ in $(10)_1$, which is the only term depending on ξ^2 and ξ^3, while $\mathbf{B}, \mathbf{D}$, and $\bar{\mathbf{S}}_t$ are constant within the section, we obtain

$$\bar{\mathbf{E}}_t^0 = -\mathbf{B}^{00\mathrm{T}} \bar{E}_{11}^0 - \mathbf{B}^{10\mathrm{T}} \bar{E}_{11}^1 - \mathbf{B}^{01\mathrm{T}} \bar{E}_{11}^2 - \mathbf{B}^{11\mathrm{T}} \bar{E}_{11}^3 + \mathbf{D}^{00} \bar{\mathbf{S}}_t. \tag{34}$$

Thus, by solving for $\bar{\mathbf{S}}_t$, we derive

$$\bar{\mathbf{S}}_t = (\mathbf{D}^{00})^{-1} \mathbf{B}^{00\mathrm{T}} \bar{E}_{11}^0 + (\mathbf{D}^{00})^{-1} \mathbf{B}^{10\mathrm{T}} \bar{E}_{11}^1 + (\mathbf{D}^{00})^{-1} \mathbf{B}^{01\mathrm{T}} \bar{E}_{11}^2 + (\mathbf{D}^{00})^{-1} \mathbf{B}^{11\mathrm{T}} \bar{E}_{11}^3 + (\mathbf{D}^{00})^{-1} \bar{\mathbf{E}}_t^0, \tag{35}$$

where $\mathbf{B}^{hk} = \int_{-1}^{1}\int_{-1}^{1} \mathbf{B}(\xi^2)^h(\xi^3)^k \mathrm{d}\xi^2\mathrm{d}\xi^3$ (with $h,k = \{0,1,2\}$) is evaluated analytically within the section. We remark that the same notation such that $(.)^{hk}$ denotes a term of order h and k along ξ^2 and ξ^3, respectively, is also used for $\mathbf{D}^{hk}$. Then, we compute the axial stress resultant by evaluating $\bar{\mathcal{N}}^k$ coefficients in Eq. (23), once substituted the constitutive relations (30), obtaining

$$\begin{bmatrix}\bar{\mathcal{N}}^0\\ \bar{\mathcal{N}}^1\\ \bar{\mathcal{N}}^2\\ \bar{\mathcal{N}}^3\end{bmatrix} = \frac{1}{4}\int_{-1}^{1}\int_{-1}^{1}\begin{bmatrix} A & \mathbf{B}\\ \xi^2 A & \xi^2\mathbf{B}\\ \xi^3 A & \xi^3\mathbf{B}\\ \xi^2\xi^3 A & \xi^2\xi^3\mathbf{B}\end{bmatrix}\begin{bmatrix}\bar{E}^0_{11}+\xi^2\bar{E}^1_{11}+\xi^3\bar{E}^2_{11}+\xi^2\xi^3\bar{E}^3_{11}\\ \bar{\mathbf{S}}_t\end{bmatrix}\mathrm{d}\xi^2\mathrm{d}\xi^3, \tag{36}$$

and, highlighting that the transverse normal stress vector and the axial strain coefficients do not depend on ξ^2 and ξ^3, we retrieve

$$\begin{bmatrix}\bar{\mathcal{N}}^0\\ \bar{\mathcal{N}}^1\\ \bar{\mathcal{N}}^2\\ \bar{\mathcal{N}}^3\end{bmatrix} = \frac{1}{4}\int_{-1}^{1}\int_{-1}^{1}\begin{bmatrix} A & \xi^2 A & \xi^3 A & \xi^2\xi^3 A & \mathbf{B}\\ \xi^2 A & (\xi^2)^2 A & \xi^2\xi^3 A & (\xi^2)^2\xi^3 A & \xi^2\mathbf{B}\\ \xi^3 A & \xi^2\xi^3 A & (\xi^3)^2 A & \xi^2(\xi^3)^2 A & \xi^3\mathbf{B}\\ \xi^2\xi^3 A & (\xi^2)^2\xi^3 A & \xi^2(\xi^3)^2 A & (\xi^2)^2(\xi^3)^2 A & \xi^2\xi^3\mathbf{B}\end{bmatrix}\mathrm{d}\xi^2\mathrm{d}\xi^3\begin{bmatrix}\bar{E}^0_{11}\\ \bar{E}^1_{11}\\ \bar{E}^2_{11}\\ \bar{E}^3_{11}\\ \bar{\mathbf{S}}_t\end{bmatrix}. \tag{37}$$

Thus, the generalized constitutive matrix corresponding to the above mentioned stress and strain components follows as

$$\begin{bmatrix}\bar{\mathcal{N}}^0\\ \bar{\mathcal{N}}^1\\ \bar{\mathcal{N}}^2\\ \bar{\mathcal{N}}^3\end{bmatrix} = \begin{bmatrix} A^{00} & A^{10} & A^{01} & A^{11} & \mathbf{B}^{00}\\ A^{10} & A^{20} & A^{11} & A^{21} & \mathbf{B}^{10}\\ A^{01} & A^{11} & A^{02} & A^{12} & \mathbf{B}^{01}\\ A^{11} & A^{21} & A^{12} & A^{22} & \mathbf{B}^{11}\end{bmatrix}\begin{bmatrix}\bar{E}^0_{11}\\ \bar{E}^1_{11}\\ \bar{E}^2_{11}\\ \bar{E}^3_{11}\\ \bar{\mathbf{S}}_t\end{bmatrix} \tag{38}$$

and its explicit form, that can be evaluated analytically at the beginning of the analysis entailing a substantial reduction of the computational effort, reads

$$\begin{bmatrix}\bar{\mathcal{N}}^0\\ \bar{\mathcal{N}}^1\\ \bar{\mathcal{N}}^2\\ \bar{\mathcal{N}}^3\\ \bar{\mathbf{S}}_t\end{bmatrix} = \underbrace{\begin{bmatrix} (A^{00}+\mathbf{B}^{00}(\mathbf{D}^{00})^{-1}\mathbf{B}^{00\mathrm{T}}) & (A^{10}+\mathbf{B}^{00}(\mathbf{D}^{00})^{-1}\mathbf{B}^{10\mathrm{T}}) & (A^{01}+\mathbf{B}^{00}(\mathbf{D}^{00})^{-1}\mathbf{B}^{01\mathrm{T}}) & (A^{11}+\mathbf{B}^{00}(\mathbf{D}^{00})^{-1}\mathbf{B}^{11\mathrm{T}}) & \mathbf{B}^{00}(\mathbf{D}^{00})^{-1}\\ (A^{10}+\mathbf{B}^{10}(\mathbf{D}^{00})^{-1}\mathbf{B}^{00\mathrm{T}}) & (A^{20}+\mathbf{B}^{10}(\mathbf{D}^{00})^{-1}\mathbf{B}^{10\mathrm{T}}) & (A^{11}+\mathbf{B}^{10}(\mathbf{D}^{00})^{-1}\mathbf{B}^{01\mathrm{T}}) & (A^{21}+\mathbf{B}^{10}(\mathbf{D}^{00})^{-1}\mathbf{B}^{11\mathrm{T}}) & \mathbf{B}^{10}(\mathbf{D}^{00})^{-1}\\ (A^{01}+\mathbf{B}^{01}(\mathbf{D}^{00})^{-1}\mathbf{B}^{00\mathrm{T}}) & (A^{11}+\mathbf{B}^{01}(\mathbf{D}^{00})^{-1}\mathbf{B}^{10\mathrm{T}}) & (A^{02}+\mathbf{B}^{01}(\mathbf{D}^{00})^{-1}\mathbf{B}^{01\mathrm{T}}) & (A^{12}+\mathbf{B}^{01}(\mathbf{D}^{00})^{-1}\mathbf{B}^{11\mathrm{T}}) & \mathbf{B}^{01}(\mathbf{D}^{00})^{-1}\\ (A^{11}+\mathbf{B}^{11}(\mathbf{D}^{00})^{-1}\mathbf{B}^{00\mathrm{T}}) & (A^{21}+\mathbf{B}^{11}(\mathbf{D}^{00})^{-1}\mathbf{B}^{10\mathrm{T}}) & (A^{12}+\mathbf{B}^{11}(\mathbf{D}^{00})^{-1}\mathbf{B}^{01\mathrm{T}}) & (A^{22}+\mathbf{B}^{11}(\mathbf{D}^{00})^{-1}\mathbf{B}^{11\mathrm{T}}) & \mathbf{B}^{11}(\mathbf{D}^{00})^{-1}\\ (\mathbf{D}^{00})^{-1}\mathbf{B}^{00\mathrm{T}} & (\mathbf{D}^{00})^{-1}\mathbf{B}^{10\mathrm{T}} & (\mathbf{D}^{00})^{-1}\mathbf{B}^{01\mathrm{T}} & (\mathbf{D}^{00})^{-1}\mathbf{B}^{11\mathrm{T}} & (\mathbf{D}^{00})^{-1}\end{bmatrix}}_{\bar{\mathbf{C}}_{\mathcal{N}}}\begin{bmatrix}\bar{E}^0_{11}\\ \bar{E}^1_{11}\\ \bar{E}^2_{11}\\ \bar{E}^3_{11}\\ \bar{\mathbf{E}}^0_t\end{bmatrix}. \tag{39}$$

Furthermore, the part of generalized constitutive matrix corresponding to the shear generalized stresses, $\bar{\mathbf{C}}_{\mathcal{T}}$, is reported, even if not treated, for completeness as

$$\begin{bmatrix}\bar{\boldsymbol{\mathcal{T}}}^0\\ \bar{\boldsymbol{\mathcal{T}}}^1\\ \bar{\boldsymbol{\mathcal{T}}}^2\\ \bar{\boldsymbol{\mathcal{T}}}^3\end{bmatrix} = \underbrace{\frac{1}{4}\int_{-1}^{1}\int_{-1}^{1}\begin{bmatrix}\bar{\mathbf{C}}_s & \xi^2\bar{\mathbf{C}}_s & \xi^3\bar{\mathbf{C}}_s & \xi^2\xi^3\bar{\mathbf{C}}_s\\ \xi^2\bar{\mathbf{C}}_s & (\xi^2)^2\bar{\mathbf{C}}_s & \xi^2\xi^3\bar{\mathbf{C}}_s & (\xi^2)^2\xi^3\bar{\mathbf{C}}_s\\ \xi^3\bar{\mathbf{C}}_s & \xi^2\xi^3\bar{\mathbf{C}}_s & (\xi^3)^2\bar{\mathbf{C}}_s & \xi^2(\xi^3)^2\bar{\mathbf{C}}_s\\ \xi^2\xi^3\bar{\mathbf{C}}_s & (\xi^2)^2\xi^3\bar{\mathbf{C}}_s & \xi^2(\xi^3)^2\bar{\mathbf{C}}_s & (\xi^2)^2(\xi^3)^2\bar{\mathbf{C}}_s\end{bmatrix}\mathrm{d}\xi^2\mathrm{d}\xi^3}_{\bar{\mathbf{C}}_{\mathcal{T}}}\begin{bmatrix}\bar{\mathbf{E}}^0_s\\ \bar{\mathbf{E}}^1_s\\ \bar{\mathbf{E}}^2_s\\ \bar{\mathbf{E}}^3_s\end{bmatrix}, \tag{40}$$

where $\bar{\mathbf{C}}_s = \begin{bmatrix}\bar{\mathbb{C}}^{2323} & \bar{\mathbb{C}}^{2313}\\ \bar{\mathbb{C}}^{1323} & \bar{\mathbb{C}}^{1313}\end{bmatrix}$ collects the coefficients corresponding to the shear strains. Finally, we can introduce the modified constitutive model

$$\bar{\mathbf{t}} = \bar{\mathbf{C}}_\rho\bar{\boldsymbol{\rho}}, \tag{41}$$

by introducing the new constitutive matrix $\bar{\mathbf{C}}_\rho$

$$\bar{\mathbf{C}}_\rho = \begin{bmatrix}\bar{\mathbf{C}}_{\mathcal{N}} & \mathbf{0}\\ \mathbf{0} & \bar{\mathbf{C}}_{\mathcal{T}}\end{bmatrix} \tag{42}$$

and the generalized stresses $\bar{\mathbf{t}}$ and strains $\bar{\boldsymbol{\rho}}$,

$$\bar{\mathbf{t}} = \begin{bmatrix}\bar{\mathcal{N}}^0 & \bar{\mathcal{N}}^1 & \bar{\mathcal{N}}^2 & \bar{\mathcal{N}}^3 & \bar{\mathbf{S}}_t & \bar{\boldsymbol{\mathcal{T}}}^0 & \bar{\boldsymbol{\mathcal{T}}}^1 & \bar{\boldsymbol{\mathcal{T}}}^2 & \bar{\boldsymbol{\mathcal{T}}}^3\end{bmatrix}^{\mathrm{T}}, \tag{43}$$

$$\bar{\boldsymbol{\rho}} = \begin{bmatrix}\bar{E}^0_{11} & \bar{E}^1_{11} & \bar{E}^2_{11} & \bar{E}^3_{11} & \bar{\mathbf{E}}^0_t & \bar{\mathbf{E}}^0_s & \bar{\mathbf{E}}^1_s & \bar{\mathbf{E}}^2_s & \bar{\mathbf{E}}^3_s\end{bmatrix}^{\mathrm{T}}. \tag{44}$$

Finally, we remark that the local Cartesian generalized strains, $\bar{\boldsymbol{\rho}}$, in Eq. (41) are obtained from the covariant ones, $\boldsymbol{\rho}$, *via* the following mapping

$$\bar{\boldsymbol{\rho}} = \mathbf{T}_\rho\boldsymbol{\rho}, \tag{45}$$

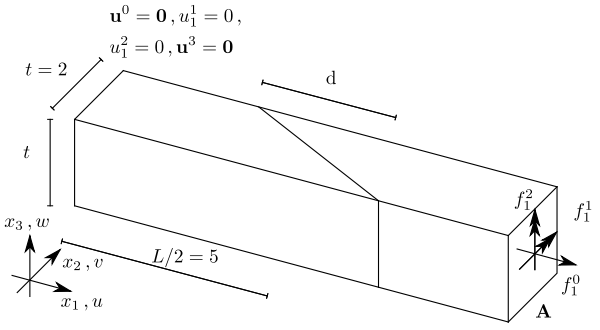

Fig. 2. Mesh distortion tests: geometry and boundary conditions.

where the explicit expression of $\mathbf{T}_\rho$ and its evaluation procedure is given in Appendix A. Additionally, in Appendix C we provide a flowchart that illustrates a step-by-step procedure to analytically evaluate the generalized constitutive matrix (42).

4.2. Membrane, shear, and curvature-thickness locking mitigation strategy with a focus on efficiency

Efficient IGA models should exploit all the features of the method mainly related to the high continuity of the shape functions. In this respect, both the quadrature rule and strategies to deal with locking should be patch-wise [2,66,74,82]. Therefore, in our work shear and membrane locking are resolved by exploiting the concept of patch-wise reduced integration and selecting the proper approximation space [74]. Here cubic C^2 NURBS and the S_1^4 approximation space [2] are employed, which will prove to tackle both shear and membrane locking entailing high efficiency at the same time due to the lower number of needed integration points with respect to the classical element-wise Gaussian integration rule.

Not only does the interpolation locking affect the efficiency of nonlinear models, it has been proven in [53,73,76] that the classical approaches in nonlinear analysis perform even better when formulated as a mixed form. Moreover, in the context of IGA efficiency-related arguments discourage the use of continuous interpolations for strains/stresses in favor of the so-called MIP [75,83] approaches. Additionally, the use of an isogeometric framework naturally alleviates curvature-thickness locking. In fact, this numerical pathology automatically arises in the case of a linear discretization of a curved geometry as the directors cannot be perpendicular to the exact solid-beam geometry. However, utilizing a higher IGA discretization along the solid-beams axis, we are able to provide the exact representation of a curved beam geometry.

5. Numerical results

In this Section, we first test the robustness of the proposed formulation by considering mesh distortion sensitivity benchmarks with respect to bending about the solid beam's cross-section parametric coordinates and the ability of the formulation to exactly represent a constant axial stress state. Then, various numerical tests are presented to showcase the performance of the introduced solid-beam formulation in the linear and geometrically nonlinear case. For all considered benchmarks, a cubic polynomial degree in the axial direction of the beam with maximum continuity order (i.e., C^2) is utilized if not otherwise specified (see Section 4.2).

5.1. Cantilever beam

5.1.1. Patch and mesh distortion sensitivity tests

The first example considers a well-established benchmark in the literature (see, e.g., [36,41,51]) to investigate the sensitivity of the proposed solid beam to mesh distortion, parametrized by the distance d as depicted in Fig. 2. This test utilizes Young's modulus $E = 1500$ and Poisson's ratio $\nu = 0$, whereas the structure is discretized by only two elements with C^0-continuity across the distorted section. The analysis is performed by considering at the free-end of the cantilever beam first an axial force $f_1^0 = 1$ and then two loads corresponding to the couples about x_2 and x_3, i.e., $f_1^1 = f_1^2 = -40$, separately. The first test aims at investigating the model's ability to reproduce a constant stress state even for distorted meshes, as depicted in Fig. 3(a). This property is crucial because it allows to verify the consistency and robustness of a finite element formulation, offering at least a necessary condition to evaluate convergence while refining the mesh.

To analyze instead the model's bending response, we study in Fig. 3(b) the horizontal and vertical tip deflections $\tilde{v}_A$ and $\tilde{w}_A$ (normalized with respect to the reference solution [36], namely $\tilde{v}_A = v_A/v_{A,ref}$, $\tilde{w}_A = w_A/w_{A,ref}$, with $v_{A,ref} = w_{A,ref} = 1$) for an increasing mesh distortion parameter d. It is possible to observe that, for the deflection v, the proposed element performs similarly (up to a reasonable level of distortion) to the Q1STb element in [36] where the authors assume either a constant Taylor expansion of the Jacobian (see "J const" nomenclature in Fig. 3(b)) or an expansion up to linear parts (i.e., "J lin"). On the contrary, while bending about x_2 axis, the proposed element performs much better in capturing the behavior of the deflection w with respect to the Q1STb element of [36]. We highlight that the proposed formulation allows to apply boundary conditions in a more straightforward

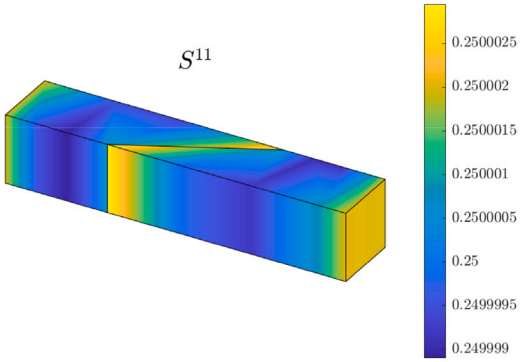

(a) Constant stress patch test.

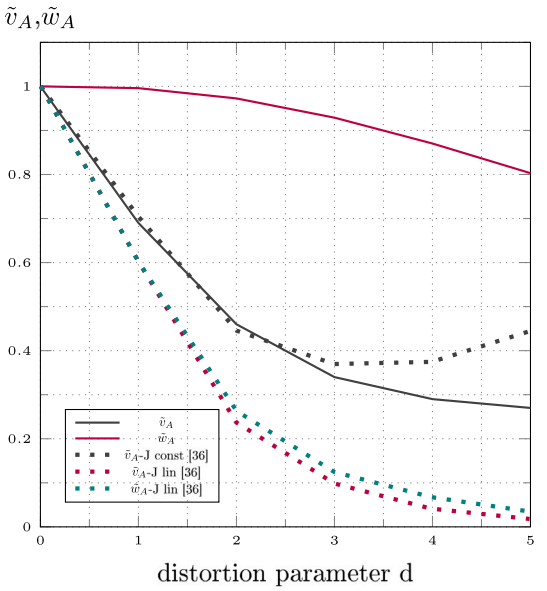

(b) Mesh distortion sensitivity tests with respect to bending.

Fig. 3. Mesh distortion tests: constant stress distribution for a fixed distortion parameter d = 2 (left). In-section displacements normalized to the reference solution in [36] (namely, $\tilde{v}_A = v_A/v_{A,ref}$, $\tilde{w}_A = w_A/w_{A,ref}$, with $v_{A,ref} = w_{A,ref} = 1$) as a function of d (right).

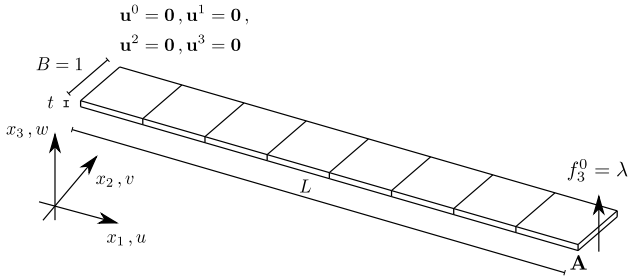

Fig. 4. Cantilever beam under shear: geometry and boundary conditions.

manner (like for exact beam models) compared with a classical 3D formulation such as the one in [36]. In particular, the rigid body motion is restrained by fixing $\mathbf{u}^0$ and the first components of the vectors $\mathbf{u}^1$ and $\mathbf{u}^2$. Similarly, our formulation allows to directly represent the bending moments about x_2 and x_3 by imposing at the solid-beam free-end the forces that are work-conjugate to the restrained displacements at $x_1 = 0$.

5.1.2. Cantilever beam under shear and compression load cases

Membrane locking can affect the solution even for straight geometries in case of large displacement analysis. A simple but highly challenging test to check locking effects concerns the cantilever beam, depicted in Fig. 4, that is analyzed under transverse loads, for two different values of the slenderness $L/t = \{100, 1000\}$, where $L = 10$ and t are the length and thickness of the solid beam, respectively, whereas $B = 1$.

To study the performance of the proposed model against shear and membrane locking under large displacements, as well as against Poisson-thickness locking, the beam is studied considering a non-zero Poisson's ratio, taking as reference the results reported in [80] for $L/t = 100$ where a solid-shell model employs a selective reduced integration of the volumetric term. As [80] does not provide results for $L/t = 1000$, we consider as reference the solid-shell solution in [35]. Therefore, in Figs. 5 and 6, we showcase the equilibrium paths for the beam subjected to the shear force λ, normalized with respect to $\lambda_{\max} = 1$ (i.e., $\tilde{\lambda} = \lambda/\lambda_{\max}$) and $E = \frac{2.1L^2}{t^3}$. Namely, Fig. 5 highlights that locking effects are resolved and the model performs well for every examined Poisson's ratio value.

According to beam theory, Poisson's ratio does not have influence on the solution. Therefore, the present solid-beam and solid-shell [35] solutions with $\nu = 0.499$ and $\nu = 0$ are expected to be almost identical. Namely, in the case of $L/t = 1000$, displayed in Fig.

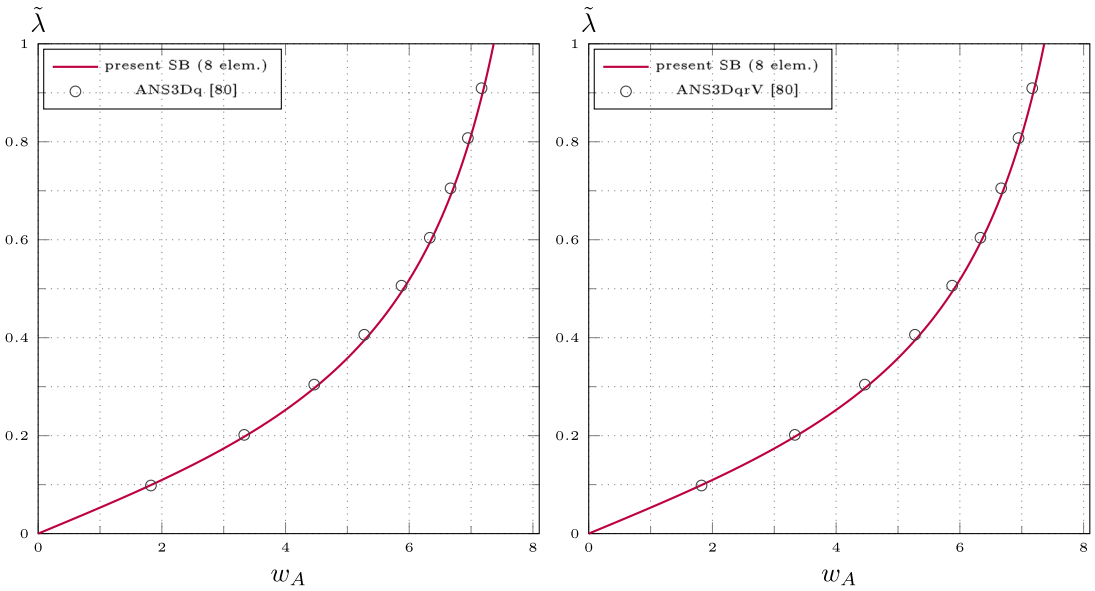

Fig. 5. Cantilever beam under shear force: equilibrium path for $L/t = 100$ and varying Poisson's ratio.

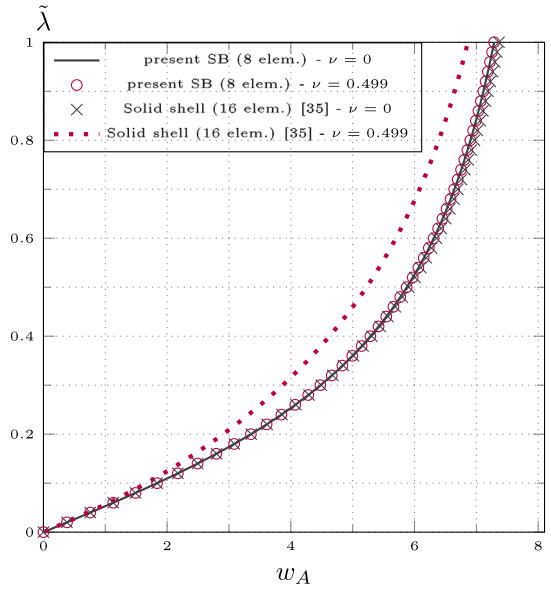

Fig. 6. Cantilever beam under shear force: equilibrium path for $L/t = 1000$ and varying Poisson's ratio.

6, the solid-shell [35] solution with $\nu = 0.499$ exhibits still volumetric locking, which, remarkably, does not occur for the proposed solid-beam formulation.

A similar study is carried out for the case of compression examined in Fig. 7, considering also a small load imperfection $f_3^0 = \epsilon\lambda$ (with $\epsilon = 1/1000$) in the transverse direction and $E = 10^7$. Figs. 8 and 9 depict the structure equilibrium paths plotting the load λ normalized with respect the analytical buckling load λ_b (namely, $\bar{\lambda} = \lambda/\lambda_b$) and prove the correctness of the proposed beam model for different values of Poisson's ratio and slenderness $L/t = \{100, 1000\}$.

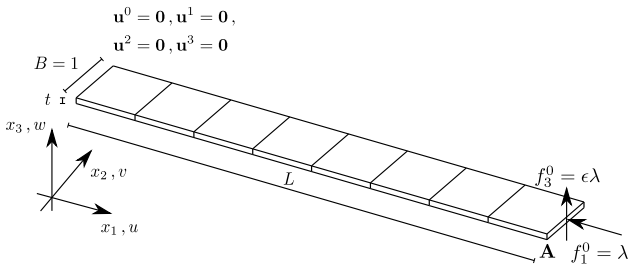

Fig. 7. Cantilever beam under compression and transverse imperfection: geometry and boundary conditions.

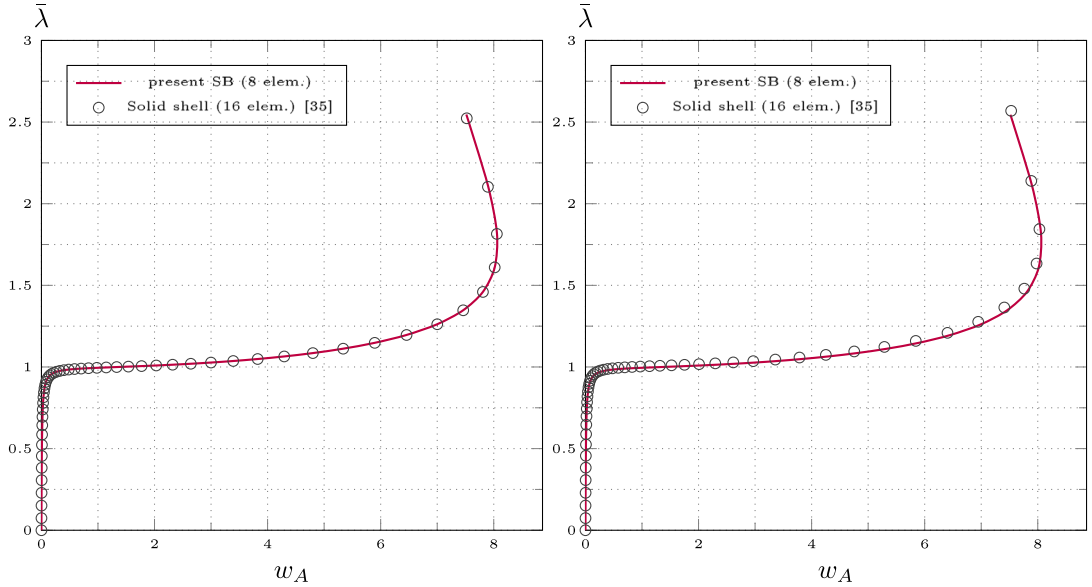

Fig. 8. Cantilever beam under compression and transverse imperfection: equilibrium path for $L/t = 100$ and varying Poisson's ratio.

5.2. 45°-arc elastic cantilever beam

We consider a 45°-arc elastic cantilever beam, as depicted in Fig. 10, that results in a challenging problem due to the coupled bending-torsion behavior. This example has been investigated in e.g., [36] and assumes a linear elastic material with $E = 10^7$ and $\nu = 0$. The cross-section is a square with a unit side (t = b = 1) and the beam is modeled with 4 and 8 elements, respectively. The analysis is performed by running the nonlinear solver at first with 1 and, then, 20 equidistant load steps up to the maximum load. Two load cases, namely $F = 300$ and $F = 600$, are analyzed and the displacement tip results are shown in Tables 1 and 2, while the equilibrium path of the displacement tip is shown in Fig. 11. The comparisons shown in Tables 1 and 2, respectively, underline the effectiveness of the MIP-based nonlinear algorithm in the case of the present solid-beam model. The accuracy of the formulation is also shown (see Fig. 11, Tables 1 and 2) in comparison with state-of-the-art references.[4,5] Additionally, in Fig. 12 we provide the bending moment profiles along the beam's axis coordinate ξ^1, highlighting that, in the case of a curved beam subjected to an out of plane load, we can appreciate the 3-D behavior of the structure as both bending moments around ξ^2 and ξ^3 directions are activated.

[4] Choi et al. (M) [84] stands for isogeometric mixed formulation with "loc-ur" and EAS, having degs = (4, 2, 2) and nel = 80 × 1 × 1, where degs denotes the degrees of the basis functions, and nel the number of elements, respectively along the axial and two transverse directions, while Choi et al. (B) [84] considers isogeometric brick elements with degs = (3, 2, 2) and nel = 320 × 1 × 1.

[5] Results taken from [6] consider two different choices of rotation parameters, namely 3- and 2-node elements. The 2-node element results are reported in brackets.

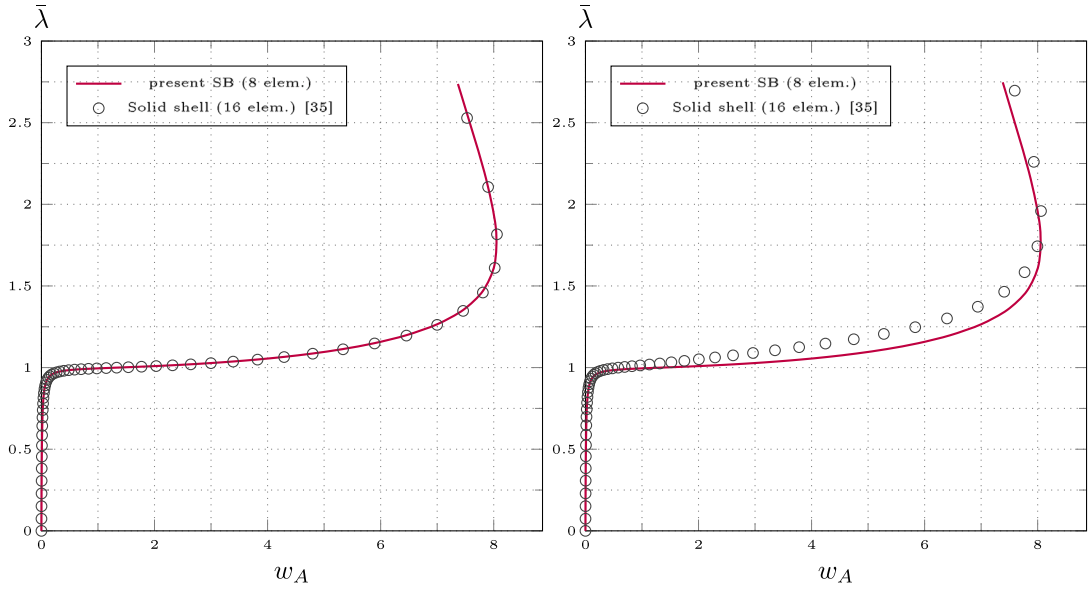

(a) $\nu = 0.$ (b) $\nu = 0.3.$

Fig. 9. Cantilever beam under compression and transverse imperfection: equilibrium path for $L/t = 1000$ and varying Poisson's ratio.

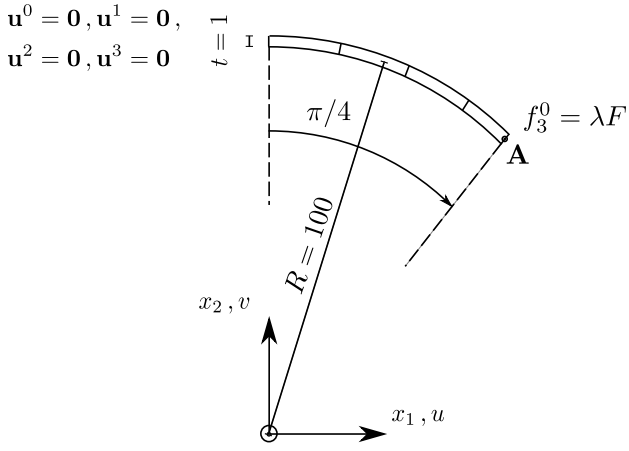

Fig. 10. 45°-arc elastic cantilever beam: geometry and boundary conditions.

Table 1
45°-arc elastic cantilever beam: tip displacements for two different load levels considering a single-step analysis and 4 SB elements.

Model	F=300				F=600			
	loops	u	v	w	loops	u	v	w
present SB	4	−11.941181	7.043669	40.146178	5	−23.548672	13.603277	53.257190
Shafqat [38]	7	−11.81	7.08	40.02	8	−23.26	13.67	53.14
Choi et al. (B) [84]	–	–	–	–	–	−23.567644	13.604269	53.477296
Choi et al. (M) [84]	–	–	–	–	–	−23.567616	13.604256	53.477273
Dvorkin et al. [85]	–	–	–	–	–	−23.50	13.60	53.30
Rhim and Lee [86]	8	−12.03	7.13	40.31	17	−23.64	13.70	53.46
Reese [36]	14	−11.71	7.27	40.06	19	−23.38	14.11	53.50
Magisano et al. [87]	–	–	–	–	–	–	–	53.475
Ibrahimbegovic [6]	–	–	–	–	–	23.557 (23.477)	13.601 (13.490)	53.467 (53.370)

Table 2
45°-arc elastic cantilever: tip displacements for two different load levels considering a single-step analysis and 8 SB elements.

model	F=300				F=600			
	loops	u	v	w	loops	u	v	w
present SB	4	−11.933228	7.044698	40.191212	5	−23.561527	13.605436	53.468926
Shafqat [38]	7	−11.81	7.08	40.02	8	−23.26	13.67	53.14
Dvorkin et al. [85]	–	–	–	–	–	−23.50	13.60	53.30
Rhim and Lee [86]	8	−12.03	7.13	40.31	17	−23.64	13.70	53.46
Reese [36]	14	−11.71	7.27	40.06	19	−23.38	14.11	53.50
Choi et al. (B) [84]	–	–	–	–	–	−23.567644	13.604269	53.477296
Choi et al. (M) [84]	–	–	–	–	–	−23.567616	13.604256	53.477273
Magisano et al. [87]	–	–	–	–	–	–	–	53.475
Ibrahimbegovic [6]	–	–	–	–	–	23.557 (23.477)	13.601 (13.490)	53.467 (53.370)

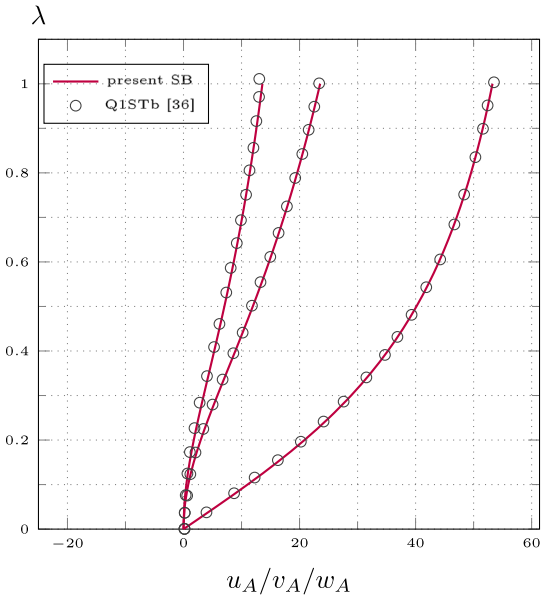

Fig. 11. 45°-arc elastic cantilever: equilibrium path for F = 600, 20 load steps, and 8 cubic elements (u_A(step = 20) = −23.548672, v_A(step = 20) = 13.603277, w_A(step = 20) = 53.25719).

5.3. Hinged deep arch

The hinged circular arch subjected to a central point load $P = \frac{EI}{R^2}$, shown in Fig. 13, considers radius $R = 100$ and a unit square cross-section. An isotropic material with Young's modulus $E = 10^6$ and shear modulus $G = 3.8\times10^5$ is examined. As it is well-known, the structure exhibits a bifurcation and a limit point along the nonlinear path. The nonlinear equilibrium paths for 8 and 16 equally spaced elements are shown in Fig. 14 and traced until the applied force P vanishes after the snap-through of the arch, which is in agreement with the solutions proposed in [86,88], whereas the calculated limit point is $\lambda_L = 15.2$, corresponding to the analytical value given in [89].

5.4. Hinged-clamped deep arch

The hinged-clamped circular arch shown in Fig. 15 is subjected to a downward point load $P = \frac{EI}{R^2}$ at the top of its extrados. The radius $R = 100$ and the cross-section is a unit square, whereas the isotropic linear elastic material properties consider Young's modulus $E = 12\times10^7$ and Poisson's ratio $\nu = 0.3$. The arch is discretized by 20 elements and the nonlinear equilibrium path is shown in Fig. 16, that depicts limit point bucklings due to the non-symmetric boundary conditions of the arch. The postbuckling behavior of this structure is very peculiar and shows four limit points and a pair of turning points [2]. The reference solution for the first limit point is $\lambda_L = 10.31$ [86], that is in agreement with the value of 10.51 obtained with the present model, also perfectly matching with the value computed using the solid-shell model in [2]. Additionally, we highlight that the curves are virtually indistinguishable in the equilibrium path up to the first limit point.

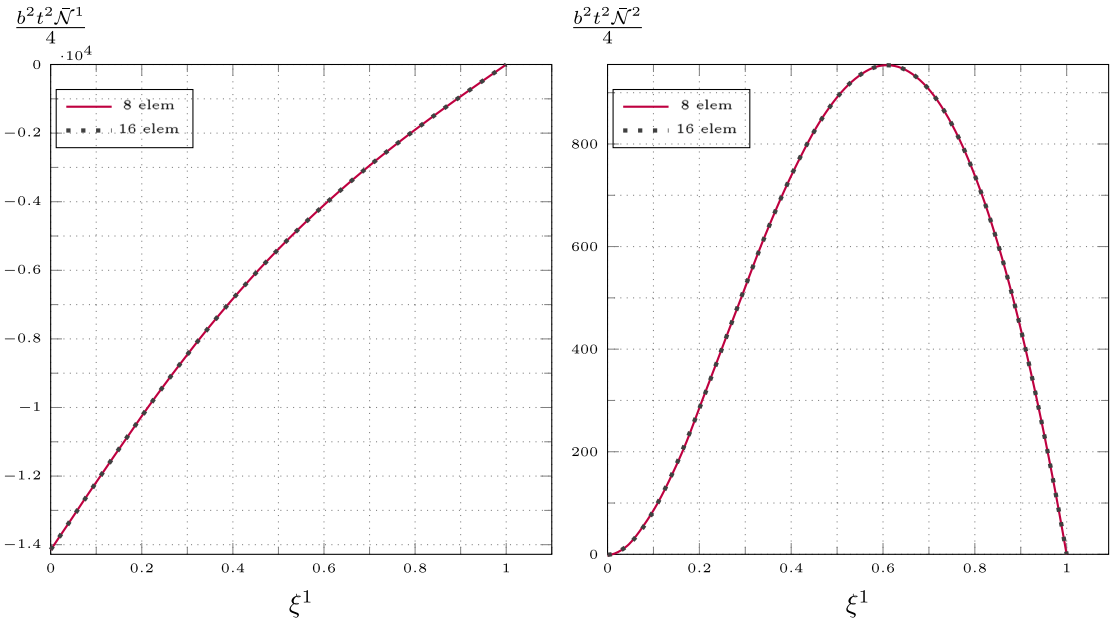

Fig. 12. 45°-arc elastic cantilever: Bending moments at last loading step for F = 600.

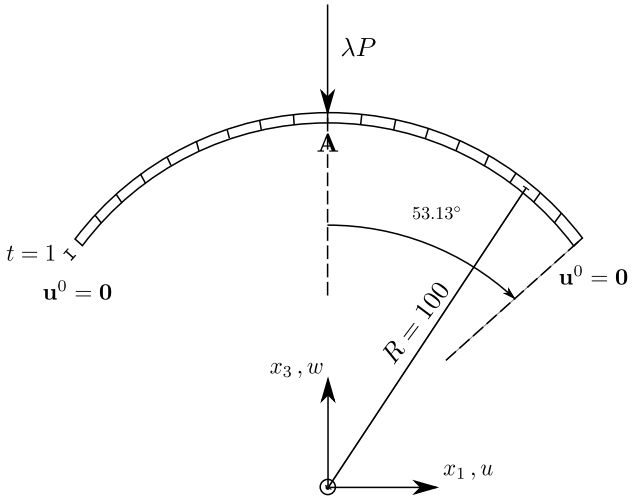

Fig. 13. Hinged deep arch: geometry and boundary conditions.

We remark that in [86], the use of the classical Hookean law yields grossly erroneous results as the authors construct a stress–strain relationship by setting to zero the off-diagonal terms of the compliance constitutive matrix. It is then possible to conclude that the difference in the equilibrium path near the turning point is due to the plane stress enforcement in the constitutive law.

5.5. Lateral buckling of a right-angle frame

This benchmark is used to test the stability of a right-angle frame and has been first proposed in [4] using beam elements and recently in the context of IGA in [38]. The geometry, boundary conditions, and discretization of the frame are shown in Fig. 17. Specifically, the structure is clamped at one end and is subject to an in-plane load λ in x_1-direction at the free-end. In order to activate the lateral buckling of the frame, an out-of-plane perturbation load $\epsilon = 0.001$ in x_2-direction is considered, whereas a linear isotropic Kirchhoff-St. Venant material model with $E = 71240$ and $\nu = 0.31$ and constant width $B = 0.6$ are examined. It is possible to observe in Fig. 18 that the proposed model (termed present SB) is in optimum agreement with the reference result, while the formulation proposed in [38] with the same degrees of approximation (i.e., ISB3) exhibits still locking effects and is not able to capture the buckling load correctly.

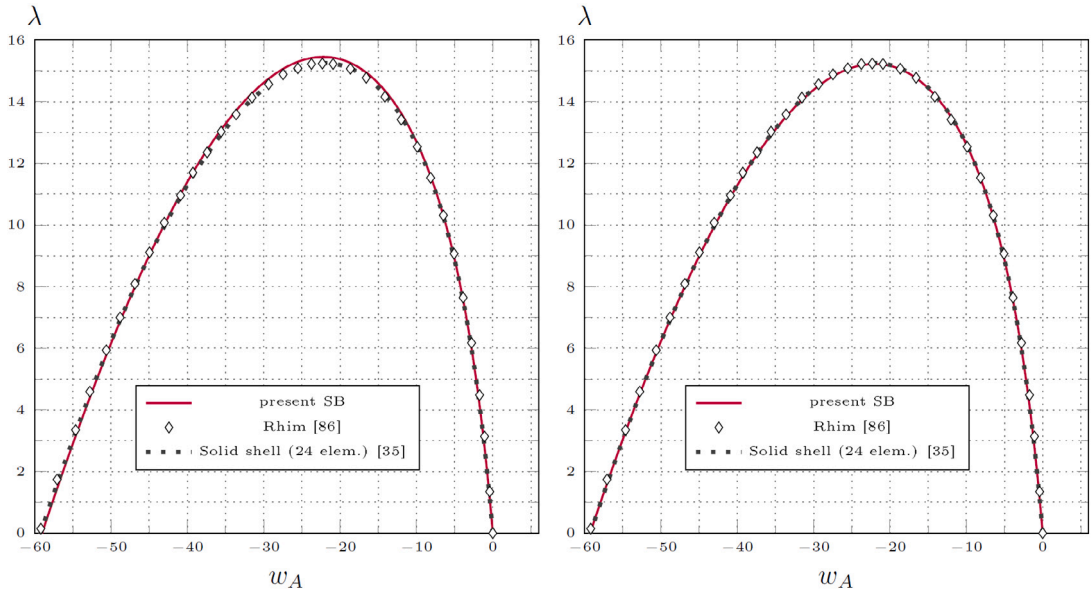

Fig. 14. Hinged deep arch: equilibrium path for 8 (left) and 16 (right) cubic SB elements.

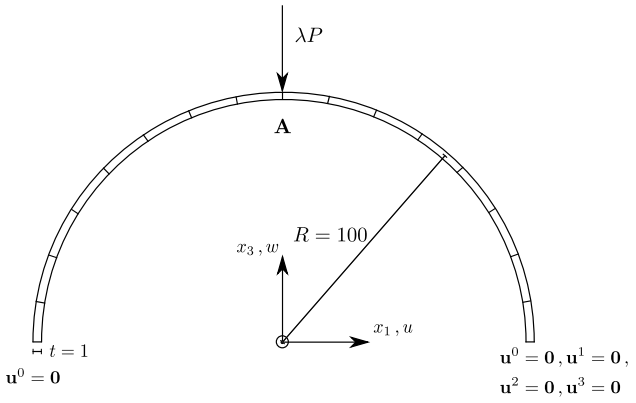

Fig. 15. Hinged-clamped deep arch: geometry and boundary conditions.

6. Conclusions

In this work, we propose a novel 12-parameter solid beam in an isogeometric framework. The geometry as well as the displacement field are completely described by a polynomial expansion that is a bilinear combination of coefficients, function of the beam's axis coordinate only, and the cross-section coordinates up to a bilinear term. This allows for a simple and flexible description of the most important stress states, which are axial stress, bending, transverse shear, and torsion and a straightforward application of boundary conditions. To resolve Poisson-thickness locking we modify the constitutive material behavior such that the stresses in both thickness directions are independent of the width and thickness coordinates, providing exact integration of the constitutive matrix within the cross-section. A precise representation of the local Cartesian strains is crucial for this operation, and is obtained by appropriately expanding the Jacobian matrix without spurious terms. By exploiting the concept of patch-wise reduced integration, namely employing cubic (C^2) isogeometric shape functions in a S_1^4 approximation space, shear and membrane locking are resolved with high efficiency. Furthermore, relying on the highly continuous properties of IGA shape functions for the discretization of the beam's axis, naturally alleviates curvature-thickness locking. The effectiveness of the suggested formulation is evaluated through a comprehensive selection of linear and geometrically nonlinear problems. Among future works, we plan to extend the current formulation to study nonlinear constitutive materials such as hyperelasticity, and capitalize on the capability of the present model to geometrically describe the beam's cross-section, taking into account the coupling with other structures and a seamless integration of contact. Additionally, the present framework will be tested in dynamic or time-dependent problems.

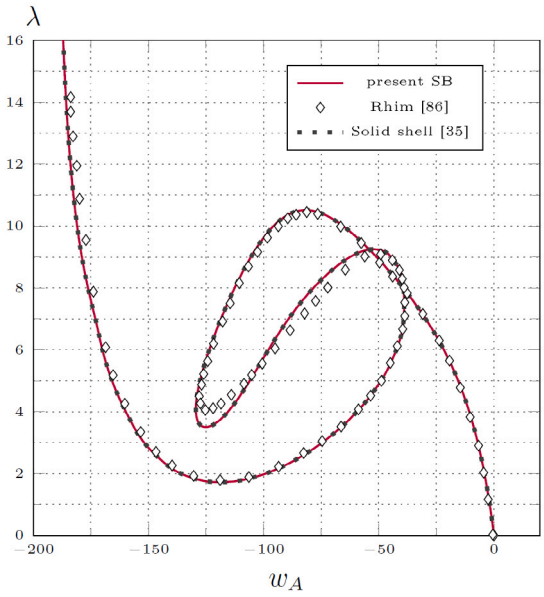

Fig. 16. Hinged-clamped deep arch: equilibrium path obtained with 20 cubic SB elements.

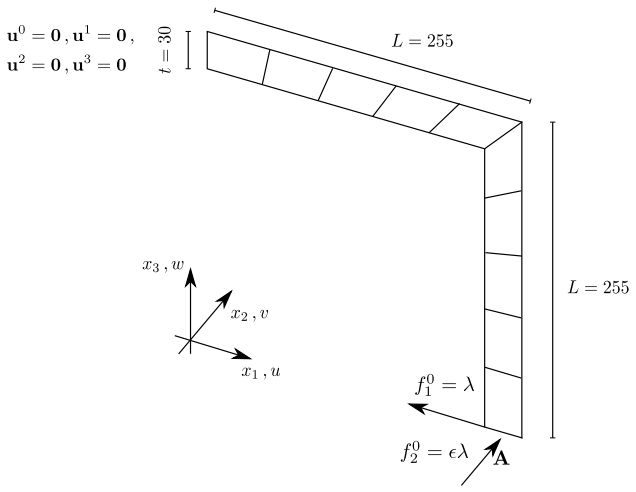

Fig. 17. Right-angle frame: geometry and boundary conditions.

CRediT authorship contribution statement

Leonardo Leonetti: Writing – review & editing, Writing – original draft, Visualization, Validation, Supervision, Software, Methodology, Investigation, Funding acquisition, Formal analysis, Conceptualization. **Alessia Patton:** Writing – review & editing, Writing – original draft, Visualization, Validation, Methodology, Investigation, Formal analysis, Conceptualization. **Josef Kiendl:** Writing – review & editing, Visualization, Validation, Supervision, Methodology, Funding acquisition, Conceptualization.

Declaration of competing interest

The authors declare that they have no known competing financial interests or personal relationships that could have appeared to influence the work reported in this paper.

Acknowledgments

This work was partially supported by the European Research Council through the H2020 ERC Consolidator Grant 2019 n. 864482 FDM2.

Leonardo Leonetti was partially supported by MUR-PRIN 2022 project ABYSS: Accurate simulation of Bio-hYbrid Soft Swimmers, Grant No. 2022BN3RAC, CUP: D53D23003410006, funded by European Union - Next Generation EU and also partially supported by MUR-PRIN PNRR 2022 project MEDUSA: Unveiling jellyfish bioMEchanics for the design of DUrable Soft Aquanauts, Grant No. P2022AC8H4, CUP: H53D23008540001, funded by European Union - Next Generation EU.

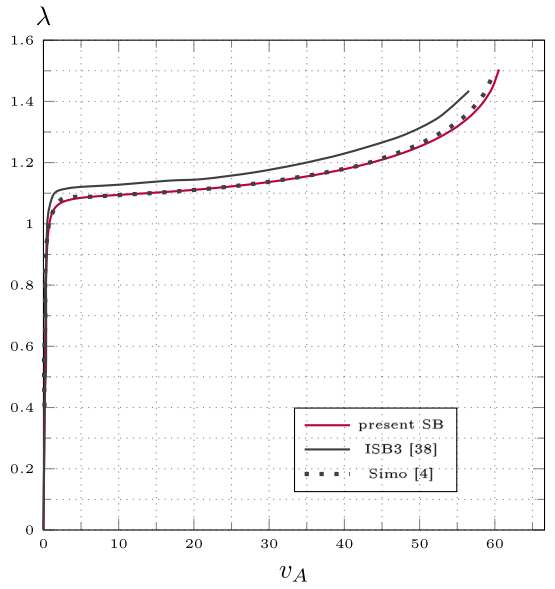

Fig. 18. Right-angle frame: equilibrium path obtained with 5+5 cubic elements. The data in [38] used for comparison have been sampled *via* the tool https://plotdigitizer.com/app.

Appendix A. Derivation of the mapping of the covariant strain into a generalized local Cartesian framework

To obtain a coherent representation of the local Cartesian strains without spurious extra terms, it is convenient to start from an analytical expression of the Jacobian to recast an appropriate mapping. Therefore, by differentiating Eq. (6), we can obtain the Jacobian in the form

$$\mathbf{J} = \mathbf{J}_0 + \xi^2\mathbf{J}_1 + \xi^3\mathbf{J}_2 + \xi^2\xi^3\mathbf{J}_3\,, \tag{A.1}$$

such that, once computing the derivatives of the position vector in the reference configuration with respect to the beam coordinates

$$\begin{aligned}
\frac{\partial\mathbf{X}}{\partial\xi^1} &= \mathbf{X}^0_{,1} + \xi^2\mathbf{X}^1_{,1} + \xi^3\mathbf{X}^2_{,1} + \xi^2\xi^3\mathbf{X}^3_{,1}\,,\\
\frac{\partial\mathbf{X}}{\partial\xi^2} &= \mathbf{X}^1 + \xi^3\mathbf{X}^3\,,\\
\frac{\partial\mathbf{X}}{\partial\xi^3} &= \mathbf{X}^2 + \xi^2\mathbf{X}^3\,,
\end{aligned}$$

we can retrieve the Jacobian expansion matrices of coefficients (A.1) as

$$\begin{aligned}
\mathbf{J}_0 &= \begin{bmatrix}\mathbf{X}^0_{,1} & \mathbf{X}^1 & \mathbf{X}^2\end{bmatrix}\,, \quad \mathbf{J}_1 = \begin{bmatrix}\mathbf{X}^1_{,1} & \mathbf{0} & \mathbf{X}^3\end{bmatrix}\,,\\
\mathbf{J}_2 &= \begin{bmatrix}\mathbf{X}^2_{,1} & \mathbf{X}^3 & \mathbf{0}\end{bmatrix}\,, \quad \mathbf{J}_3 = \begin{bmatrix}\mathbf{X}^3_{,1} & \mathbf{0} & \mathbf{0}\end{bmatrix}\,.
\end{aligned}$$

Then, the inverse Jacobian, required for the evaluation of the strain mapping, is also expressed through a bilinear expansion as

$$\mathbf{J}^{-1} = \mathbf{J}_0^{-1} + \xi^2\mathbf{J}_1^{-1} + \xi^3\mathbf{J}_2^{-1} + \xi^2\xi^3\mathbf{J}_3^{-1}\,,$$

where the coefficients of the expansion can be obtained by exploiting the identity $\mathbf{J}\mathbf{J}^{-1} = \mathbf{I}$ as follows

$$\begin{aligned}
&\mathbf{J}_0\mathbf{J}_0^{-1} + \xi^2\mathbf{J}_0\mathbf{J}_1^{-1} + \xi^3\mathbf{J}_0\mathbf{J}_2^{-1} + \xi^2\xi^3\mathbf{J}_0\mathbf{J}_3^{-1} +\\
&\xi^2\mathbf{J}_1\mathbf{J}_0^{-1} + \xi^2\xi^2\mathbf{J}_1\mathbf{J}_1^{-1} + \xi^3\xi^2\mathbf{J}_1\mathbf{J}_2^{-1} + \xi^2\xi^3\xi^2\mathbf{J}_1\mathbf{J}_3^{-1} +\\
&\xi^3\mathbf{J}_2\mathbf{J}_0^{-1} + \xi^2\xi^3\mathbf{J}_2\mathbf{J}_1^{-1} + \xi^3\xi^3\mathbf{J}_2\mathbf{J}_2^{-1} + \xi^2\xi^3\xi^3\mathbf{J}_2\mathbf{J}_3^{-1} +\\
&\xi^2\xi^3\mathbf{J}_3\mathbf{J}_0^{-1} + \xi^2\xi^3\mathbf{J}_3\xi^2\mathbf{J}_1^{-1} + \xi^2\xi^3\mathbf{J}_3\xi^3\mathbf{J}_2^{-1} + \xi^2\xi^3\mathbf{J}_3\xi^2\xi^3\mathbf{J}_3^{-1} = \mathbf{I}\,.
\end{aligned} \tag{A.2}$$

By neglecting terms of order higher than ξ^2, ξ^3 in Eq. (A.2), we obtain

$$\mathbf{J}_0\mathbf{J}_0^{-1} + \xi^2(\mathbf{J}_0\mathbf{J}_1^{-1} + \mathbf{J}_1\mathbf{J}_0^{-1}) + \xi^3(\mathbf{J}_0\mathbf{J}_2^{-1} + \mathbf{J}_2\mathbf{J}_0^{-1}) + \xi^2\xi^3(\mathbf{J}_0\mathbf{J}_3^{-1} + \mathbf{J}_1\mathbf{J}_2^{-1} + \mathbf{J}_2\mathbf{J}_1^{-1} + \mathbf{J}_3\mathbf{J}_0^{-1}) = \mathbf{I},$$

and, therefore, the set of equations

$$\begin{aligned}
&\mathbf{J}_0\mathbf{J}_0^{-1} = \mathbf{I}\,,\\
&\mathbf{J}_0\mathbf{J}_1^{-1} + \mathbf{J}_1\mathbf{J}_0^{-1} = \mathbf{0} \rightarrow \mathbf{J}_1^{-1} = -\mathbf{J}_0^{-1}\mathbf{J}_1\mathbf{J}_0^{-1}\,,\\
&\mathbf{J}_0\mathbf{J}_2^{-1} + \mathbf{J}_2\mathbf{J}_0^{-1} = \mathbf{0} \rightarrow \mathbf{J}_2^{-1} = -\mathbf{J}_0^{-1}\mathbf{J}_2\mathbf{J}_0^{-1}\,,\\
&\mathbf{J}_0\mathbf{J}_3^{-1} + \mathbf{J}_3\mathbf{J}_0^{-1} + \mathbf{J}_2\mathbf{J}_1^{-1} + \mathbf{J}_1\mathbf{J}_2^{-1} = \mathbf{0} \rightarrow \mathbf{J}_3^{-1} = -\mathbf{J}_0^{-1}(\mathbf{J}_3\mathbf{J}_0^{-1} + \mathbf{J}_2\mathbf{J}_1^{-1} + \mathbf{J}_1\mathbf{J}_2^{-1})\,.
\end{aligned}$$

For the sake of clarity, we simplify the notation and rename the inverse Jacobian expansion matrices of coefficients as $\mathbf{J}_0^{-1} = [j_{ij}]$, $\mathbf{J}_1^{-1} = [a_{ij}]$, $\mathbf{J}_2^{-1} = [b_{ij}]$, and $\mathbf{J}_3^{-1} = [c_{ij}]$. These coefficients are needed in the mapping to express the covariant strain in Voigt's notation in a local Cartesian system $\bar{\mathbf{E}} = \mathbf{T}\mathbf{E}$, such that the transformation operator $\mathbf{T}$ is consistently structured as the former Jacobian and inverse Jacobian expansions and reads

$$\mathbf{T} = \mathbf{T}^0 + \xi^2\mathbf{T}^1 + \xi^3\mathbf{T}^2 + \xi^2\xi^3\mathbf{T}^3\,,$$

where

$$\mathbf{T}^0 = \left[\frac{\partial \bar{E}^0_{ij}}{\partial E_{hk}}\right] = \begin{bmatrix}
T^0_{1111} & T^0_{1122} & T^0_{1133} & T^0_{1112} & T^0_{1123} & T^0_{1123}\\
T^0_{2211} & T^0_{2222} & T^0_{2233} & T^0_{2212} & T^0_{2223} & T^0_{2213}\\
T^0_{3311} & T^0_{3322} & T^0_{3333} & T^0_{3312} & T^0_{3323} & T^0_{3313}\\
T^0_{1211} & T^0_{1222} & T^0_{1233} & T^0_{1212} & T^0_{1223} & T^0_{1213}\\
T^0_{2311} & T^0_{2322} & T^0_{2333} & T^0_{2312} & T^0_{2323} & T^0_{2313}\\
T^0_{1311} & T^0_{1322} & T^0_{1333} & T^0_{1312} & T^0_{1323} & T^0_{1313}
\end{bmatrix}$$

$$= \begin{bmatrix}
{j_{11}}^2 & {j_{21}}^2 & {j_{31}}^2 & j_{11}j_{21} & j_{21}j_{31} & j_{11}j_{31}\\
{j_{12}}^2 & {j_{22}}^2 & {j_{32}}^2 & j_{12}j_{22} & j_{22}j_{32} & j_{12}j_{32}\\
{j_{13}}^2 & {j_{23}}^2 & {j_{33}}^2 & j_{13}j_{23} & j_{23}j_{33} & j_{13}j_{33}\\
2j_{11}j_{12} & 2j_{21}j_{22} & 2j_{31}j_{32} & j_{11}j_{22} + j_{12}j_{21} & j_{21}j_{32} + j_{22}j_{31} & j_{11}j_{32} + j_{12}j_{31}\\
2j_{12}j_{13} & 2j_{22}j_{23} & 2j_{32}j_{33} & j_{12}j_{23} + j_{13}j_{22} & j_{22}j_{33} + j_{23}j_{32} & j_{12}j_{33} + j_{13}j_{32}\\
2j_{11}j_{13} & 2j_{21}j_{23} & 2j_{31}j_{33} & j_{11}j_{23} + j_{13}j_{21} & j_{21}j_{33} + j_{23}j_{31} & j_{11}j_{33} + j_{13}j_{31}
\end{bmatrix},$$

$$\mathbf{T}^1 = \left[\frac{\partial \bar{E}^1_{ij}}{\partial E_{hk}}\right] = \begin{bmatrix}
T^1_{1111} & T^1_{1122} & T^1_{1133} & T^1_{1112} & T^1_{1123} & T^1_{1123}\\
T^1_{2211} & T^1_{2222} & T^1_{2233} & T^1_{2212} & T^1_{2223} & T^1_{2213}\\
T^1_{3311} & T^1_{3322} & T^1_{3333} & T^1_{3312} & T^1_{3323} & T^1_{3313}\\
T^1_{1211} & T^1_{1222} & T^1_{1233} & T^1_{1212} & T^1_{1223} & T^1_{1213}\\
T^1_{2311} & T^1_{2322} & T^1_{2333} & T^1_{2312} & T^1_{2323} & T^1_{2313}\\
T^1_{1311} & T^1_{1322} & T^1_{1333} & T^1_{1312} & T^1_{1323} & T^1_{1313}
\end{bmatrix}$$

$$= \begin{bmatrix}
2a_{11}j_{11} & 2a_{21}j_{21} & 2a_{31}j_{31}\\
2a_{12}j_{12} & 2a_{22}j_{22} & 2a_{32}j_{32}\\
2a_{13}j_{13} & 2a_{23}j_{23} & 2a_{33}j_{33}\\
2a_{11}j_{12} + 2a_{12}j_{11} & 2a_{21}j_{22} + 2a_{22}j_{21} & 2a_{31}j_{32} + 2a_{32}j_{31}\\
2a_{12}j_{13} + 2a_{13}j_{12} & 2a_{22}j_{23} + 2a_{23}j_{22} & 2a_{32}j_{33} + 2a_{33}j_{32}\\
2a_{11}j_{13} + 2a_{13}j_{11} & 2a_{21}j_{23} + 2a_{23}j_{21} & 2a_{31}j_{33} + 2a_{33}j_{31}
\end{bmatrix}$$

$$\begin{bmatrix}
a_{11}j_{21} + a_{21}j_{11} & a_{21}j_{31} + a_{31}j_{21} & a_{11}j_{31} + a_{31}j_{11}\\
a_{12}j_{22} + a_{22}j_{12} & a_{22}j_{32} + a_{32}j_{22} & a_{12}j_{32} + a_{32}j_{12}\\
a_{13}j_{23} + a_{23}j_{13} & a_{23}j_{33} + a_{33}j_{23} & a_{13}j_{33} + a_{33}j_{13}\\
a_{11}j_{22} + a_{12}j_{21} + a_{21}j_{12} + a_{22}j_{11} & a_{21}j_{32} + a_{22}j_{31} + a_{31}j_{22} + a_{32}j_{21} & a_{11}j_{32} + a_{12}j_{31} + a_{31}j_{12} + a_{32}j_{11}\\
a_{12}j_{23} + a_{13}j_{22} + a_{22}j_{13} + a_{23}j_{12} & a_{22}j_{33} + a_{23}j_{32} + a_{32}j_{23} + a_{33}j_{22} & a_{12}j_{33} + a_{13}j_{32} + a_{32}j_{13} + a_{33}j_{12}\\
a_{11}j_{23} + a_{13}j_{21} + a_{21}j_{13} + a_{23}j_{11} & a_{21}j_{33} + a_{23}j_{31} + a_{31}j_{23} + a_{33}j_{21} & a_{11}j_{33} + a_{13}j_{31} + a_{31}j_{13} + a_{33}j_{11}
\end{bmatrix},$$

$$\mathbf{T}^2 = \left[\frac{\partial \bar{E}^2_{ij}}{\partial E_{hk}}\right] = \begin{bmatrix} T^2_{1111} & T^2_{1122} & T^2_{1133} & T^2_{1112} & T^2_{1123} & T^2_{1123} \\ T^2_{2211} & T^2_{2222} & T^2_{2233} & T^2_{2212} & T^2_{2223} & T^2_{2213} \\ T^2_{3311} & T^2_{3322} & T^2_{3333} & T^2_{3312} & T^2_{3323} & T^2_{3313} \\ T^2_{1211} & T^2_{1222} & T^2_{1233} & T^2_{1212} & T^2_{1223} & T^2_{1213} \\ T^2_{2311} & T^2_{2322} & T^2_{2333} & T^2_{2312} & T^2_{2323} & T^2_{2313} \\ T^2_{1311} & T^2_{1322} & T^2_{1333} & T^2_{1312} & T^2_{1323} & T^2_{1313} \end{bmatrix}$$

$$= \begin{bmatrix} 2b_{11}j_{11} & 2b_{21}j_{21} & 2b_{31}j_{31} \\ 2b_{12}j_{12} & 2b_{22}j_{22} & 2b_{32}j_{32} \\ 2b_{13}j_{13} & 2b_{23}j_{23} & 2b_{33}j_{33} \\ 2b_{11}j_{12}+2b_{12}j_{11} & 2b_{21}j_{22}+2b_{22}j_{21} & 2b_{31}j_{32}+2b_{32}j_{31} \\ 2b_{12}j_{13}+2b_{13}j_{12} & 2b_{22}j_{23}+2b_{23}j_{22} & 2b_{32}j_{33}+2b_{33}j_{32} \\ 2b_{11}j_{13}+2b_{13}j_{11} & 2b_{21}j_{23}+2b_{23}j_{21} & 2b_{31}j_{33}+2b_{33}j_{31} \end{bmatrix}$$

$$\begin{bmatrix} b_{11}j_{21}+b_{21}j_{11} & b_{21}j_{31}+b_{31}j_{21} & b_{11}j_{31}+b_{31}j_{11} \\ b_{12}j_{22}+b_{22}j_{12} & b_{22}j_{32}+b_{32}j_{22} & b_{12}j_{32}+b_{32}j_{12} \\ b_{13}j_{23}+b_{23}j_{13} & b_{23}j_{33}+b_{33}j_{23} & b_{13}j_{33}+b_{33}j_{13} \\ b_{11}j_{22}+b_{12}j_{21}+b_{21}j_{12}+b_{22}j_{11} & b_{21}j_{32}+b_{22}j_{31}+b_{31}j_{22}+b_{32}j_{21} & b_{11}j_{32}+b_{12}j_{31}+b_{31}j_{12}+b_{32}j_{11} \\ b_{12}j_{23}+b_{13}j_{22}+b_{22}j_{13}+b_{23}j_{12} & b_{22}j_{33}+b_{23}j_{32}+b_{32}j_{23}+b_{33}j_{22} & b_{12}j_{33}+b_{13}j_{32}+b_{32}j_{13}+b_{33}j_{12} \\ b_{11}j_{23}+b_{13}j_{21}+b_{21}j_{13}+b_{23}j_{11} & b_{21}j_{33}+b_{23}j_{31}+b_{31}j_{23}+b_{33}j_{21} & b_{11}j_{33}+b_{13}j_{31}+b_{31}j_{13}+b_{33}j_{11} \end{bmatrix},$$

$$\mathbf{T}^3 = \left[\frac{\partial \bar{E}^3_{ij}}{\partial E_{hk}}\right] = \begin{bmatrix} T^3_{1111} & T^3_{1122} & T^3_{1133} & T^3_{1112} & T^3_{1123} & T^3_{1123} \\ T^3_{2211} & T^3_{2222} & T^3_{2233} & T^3_{2212} & T^3_{2223} & T^3_{2213} \\ T^3_{3311} & T^3_{3322} & T^3_{3333} & T^3_{3312} & T^3_{3323} & T^3_{3313} \\ T^3_{1211} & T^3_{1222} & T^3_{1233} & T^3_{1212} & T^3_{1223} & T^3_{1213} \\ T^3_{2311} & T^3_{2322} & T^3_{2333} & T^3_{2312} & T^3_{2323} & T^3_{2313} \\ T^3_{1311} & T^3_{1322} & T^3_{1333} & T^3_{1312} & T^3_{1323} & T^3_{1313} \end{bmatrix}$$

$$= \begin{bmatrix} 2a_{11}b_{11}+2c_{11}j_{11} & 2a_{21}b_{21}+2c_{21}j_{21} \\ 2a_{12}b_{12}+2c_{12}j_{12} & 2a_{22}b_{22}+2c_{22}j_{22} \\ 2a_{13}b_{13}+2c_{13}j_{13} & 2a_{23}b_{23}+2c_{23}j_{23} \\ 2a_{11}b_{12}+2a_{12}b_{11}+2c_{11}j_{12}+2c_{12}j_{11} & 2a_{21}b_{22}+2a_{22}b_{21}+2c_{21}j_{22}+2c_{22}j_{21} \\ 2a_{12}b_{13}+2a_{13}b_{12}+2c_{12}j_{13}+2c_{13}j_{12} & 2a_{22}b_{23}+2a_{23}b_{22}+2c_{22}j_{23}+2c_{23}j_{22} \\ 2a_{11}b_{13}+2a_{13}b_{11}+2c_{11}j_{13}+2c_{13}j_{11} & 2a_{21}b_{23}+2a_{23}b_{21}+2c_{21}j_{23}+2c_{23}j_{21} \end{bmatrix}$$

$$\begin{bmatrix} 2a_{31}b_{31}+2c_{31}j_{31} & \\ 2a_{32}b_{32}+2c_{32}j_{32} & a_{12}b_{22}+a_{22}b_{12}+c_{12}j_{22}+c_{22}j_{12} \\ 2a_{33}b_{33}+2c_{33}j_{33} & a_{13}b_{23}+a_{23}b_{13}+c_{13}j_{23}+c_{23}j_{13} \\ 2a_{31}b_{32}+2a_{32}b_{31}+2c_{31}j_{32}+2c_{32}j_{31} & a_{11}b_{22}+a_{12}b_{21}+a_{21}b_{12}+a_{22}b_{11}+c_{11}j_{22}+c_{12}j_{21}+c_{21}j_{12}+c_{22}j_{11} \\ 2a_{32}b_{33}+2a_{33}b_{32}+2c_{32}j_{33}+2c_{33}j_{32} & a_{12}b_{23}+a_{13}b_{22}+a_{22}b_{13}+a_{23}b_{12}+c_{12}j_{23}+c_{13}j_{22}+c_{22}j_{13}+c_{23}j_{12} \\ 2a_{31}b_{33}+2a_{33}b_{31}+2c_{31}j_{33}+2c_{33}j_{31} & a_{11}b_{23}+a_{13}b_{21}+a_{21}b_{13}+a_{23}b_{11}+c_{11}j_{23}+c_{13}j_{21}+c_{21}j_{13}+c_{23}j_{11} \end{bmatrix}$$

$$\begin{bmatrix} a_{21}b_{31}+a_{31}b_{21}+c_{21}j_{31}+c_{31}j_{21} \\ a_{22}b_{32}+a_{32}b_{22}+c_{22}j_{32}+c_{32}j_{22} \\ a_{23}b_{33}+a_{33}b_{23}+c_{23}j_{3,3}+c_{33}j_{23} \\ a_{21}b_{32}+a_{2,2}b_{31}+a_{31}b_{22}+a_{32}b_{21}+c_{21}j_{32}+c_{22}j_{31}+c_{31}j_{22}+c_{32}j_{21} \\ a_{22}b_{33}+a_{23}b_{32}+a_{32}b_{23}+a_{33}b_{22}+c_{22}j_{33}+c_{23}j_{32}+c_{32}j_{23}+c_{33}j_{22} \\ a_{21}b_{3,3}+a_{23}b_{31}+a_{31}b_{23}+a_{33}b_{21}+c_{2,1}j_{33}+c_{23}j_{31}+c_{31}j_{23}+c_{33}j_{21}j_{11} \end{bmatrix}$$

$$\begin{bmatrix} a_{11}b_{31}+a_{31}b_{11}+c_{11}j_{31}+c_{31}j_{11} \\ a_{12}b_{32}+a_{32}b_{12}+c_{12}j_{32}+c_{32}j_{12} \\ a_{13}b_{33}+a_{33}b_{13}+c_{13}j_{33}+c_{33}j_{13} \\ a_{11}b_{32}+a_{12}b_{31}+a_{31}b_{12}+a_{32}b_{11}+c_{11}j_{32}+c_{12}j_{31}+c_{31}j_{12}+c_{32}j_{11} \\ a_{12}b_{33}+a_{13}b_{32}+a_{32}b_{13}+a_{33}b_{12}+c_{12}j_{33}+c_{13}j_{32}+c_{32}j_{13}+c_{33}j_{12} \\ a_{11}b_{33}+a_{13}b_{31}+a_{31}b_{13}+a_{33}b_{11}+c_{11}j_{33}+c_{13}j_{31}+c_{31}j_{13}+c_{33}j_{11} \end{bmatrix}.$$

Finally, to describe the mapping to obtain the generalized covariant strain $\boldsymbol{\rho}$ (see Eq. (45)) in a local Cartesian system $\bar{\boldsymbol{\rho}}$, we detail $\mathbf{T}_\rho$ operator reorganizing $\mathbf{T}^0$, $\mathbf{T}^1$, $\mathbf{T}^2$, and $\mathbf{T}^3$ expansion coefficients as

$$\mathbf{T}_\rho = \left[\frac{\partial \bar{\rho}_i}{\partial \rho_j}\right] = \begin{bmatrix}
T^0_{1111} & T^0_{1123} & 0 & 0 & 0 & 0 & 0 & 0 & T^0_{1122} \\
T^0_{2311} & T^0_{2323} & 0 & 0 & 0 & 0 & 0 & 0 & T^0_{2322} \\
T^1_{1111} & T^1_{1123} & T^0_{1111} & T^0_{1123} & 0 & 0 & 0 & 0 & T^1_{1122} \\
T^1_{2311} & T^1_{2323} & T^0_{2311} & T^0_{2323} & 0 & 0 & 0 & 0 & T^1_{2322} \\
T^2_{1111} & T^2_{1123} & 0 & 0 & T^0_{1111} & T^0_{1123} & 0 & 0 & T^2_{1122} \\
T^2_{2311} & T^2_{2323} & 0 & 0 & T^0_{2311} & T^0_{2323} & 0 & 0 & T^2_{2322} \\
T^3_{1111} & T^3_{1123} & T^2_{1111} & T^2_{1123} & T^1_{1111} & T^1_{1123} & T^0_{1111} & T^0_{1123} & T^3_{1122} \\
T^3_{2311} & T^3_{2323} & T^1_{2311} & T^2_{2323} & T^1_{2311} & T^1_{2323} & T^0_{2311} & T^0_{2323} & T^3_{2322} \\
T^0_{2211} & T^0_{2223} & 0 & 0 & 0 & 0 & 0 & 0 & T^0_{2222} \\
T^0_{3311} & T^0_{3323} & 0 & 0 & 0 & 0 & 0 & 0 & T^0_{3322} \\
T^0_{1211} & T^0_{1223} & 0 & 0 & 0 & 0 & 0 & 0 & T^0_{1222} \\
T^0_{1311} & T^0_{1323} & 0 & 0 & 0 & 0 & 0 & 0 & T^0_{1322} \\
T^1_{1211} & T^1_{1223} & T^0_{1211} & T^0_{1223} & 0 & 0 & 0 & 0 & T^1_{1222} \\
T^1_{1311} & T^1_{1323} & T^0_{1311} & T^0_{1323} & 0 & 0 & 0 & 0 & T^1_{1322} \\
T^2_{1211} & T^2_{1223} & 0 & 0 & T^0_{1211} & T^0_{1223} & 0 & 0 & T^2_{1222} \\
T^2_{1311} & T^2_{1323} & 0 & 0 & T^0_{1311} & T^0_{1323} & 0 & 0 & T^2_{1322} \\
T^3_{1211} & T^3_{1223} & T^2_{1211} & T^2_{1223} & T^1_{1211} & T^1_{1223} & T^0_{1211} & T^0_{1223} & T^3_{1222} \\
T^3_{1311} & T^3_{1323} & T^2_{1311} & T^2_{1323} & T^1_{1311} & T^1_{1323} & T^0_{1311} & T^0_{1323} & T^3_{1322}
\end{bmatrix}$$

$$\begin{bmatrix}
T^0_{1133} & T^0_{1112} & T^0_{1123} & 0 & 0 & 0 & 0 & 0 & 0 \\
T^0_{2333} & T^0_{2312} & T^0_{2313} & 0 & 0 & 0 & 0 & 0 & 0 \\
T^1_{1133} & T^1_{1112} & T^1_{1123} & T^0_{1112} & T^0_{1123} & 0 & 0 & 0 & 0 \\
T^1_{2333} & T^1_{2312} & T^1_{2313} & T^0_{2312} & T^0_{2313} & 0 & 0 & 0 & 0 \\
T^2_{1133} & T^2_{1112} & T^1_{1123} & 0 & 0 & T^0_{1112} & T^0_{1123} & 0 & 0 \\
T^2_{2333} & T^2_{2312} & T^1_{2313} & 0 & 0 & T^0_{2312} & T^0_{2313} & 0 & 0 \\
T^3_{1133} & T^3_{1112} & T^1_{1123} & T^2_{1112} & T^1_{1123} & T^1_{1112} & T^1_{1123} & T^0_{1112} & T^0_{1123} \\
T^3_{2333} & T^3_{2312} & T^1_{2313} & T^2_{2312} & T^1_{2313} & T^1_{2312} & T^1_{2313} & T^0_{2312} & T^0_{2313} \\
T^0_{2233} & T^0_{2212} & T^0_{2213} & 0 & 0 & 0 & 0 & 0 & 0 \\
T^0_{3333} & T^0_{3312} & T^0_{3313} & 0 & 0 & 0 & 0 & 0 & 0 \\
T^0_{1233} & T^0_{1212} & T^0_{1213} & 0 & 0 & 0 & 0 & 0 & 0 \\
T^0_{1333} & T^0_{1312} & T^0_{1313} & 0 & 0 & 0 & 0 & 0 & 0 \\
T^1_{1233} & T^1_{1212} & T^1_{1213} & T^0_{1212} & T^0_{1213} & 0 & 0 & 0 & 0 \\
T^1_{1333} & T^1_{1312} & T^1_{1313} & T^0_{1312} & T^0_{1313} & 0 & 0 & 0 & 0 \\
T^2_{1233} & T^2_{1212} & T^1_{1213} & 0 & 0 & T^0_{1212} & T^0_{1213} & 0 & 0 \\
T^2_{1333} & T^2_{1312} & T^2_{1313} & 0 & 0 & T^0_{1312} & T^0_{1313} & 0 & 0 \\
T^3_{1233} & T^3_{1212} & T^1_{1213} & T^2_{1212} & T^1_{1213} & T^1_{1212} & T^1_{1213} & T^0_{1212} & T^0_{1213} \\
T^3_{1333} & T^3_{1312} & T^3_{1313} & T^2_{1312} & T^2_{1313} & T^1_{1312} & T^1_{1313} & T^0_{1312} & T^0_{1313}
\end{bmatrix}.$$

We remark that all symbolic computations are carried out using the software Maple [90].

Appendix B. Closed-form matrices for the discretization of the solid-beam element strain components

In Section 3.2, we highlight that both the linear and nonlinear terms of the covariant strain showcase the same structure in terms of quadratic forms at the discrete element level (see Eq. (26)). Thus, the symmetric matrix $\mathbf{Q}_{ij}$ in Eq. (27), associated to these quadratic forms, naturally follows the same polynomial expansion up to a bilinear term in the cross-section coordinates and its

coefficients $\mathbf{Q}_{ij}^{k}$ (with $k = \{0, 1, ..3\}$) are reported in the following in closed-form for the approximation of the membrane strain E_{11}

$$\mathbf{Q}_{11}^{0} = \begin{bmatrix} \left(\mathbf{N}_{,1}^{e}\right)^{\mathrm{T}}\mathbf{N}_{,1}^{e} & \mathbf{0} & \mathbf{0} & \mathbf{0} \\ \mathbf{0} & \mathbf{0} & \mathbf{0} & \mathbf{0} \\ \mathbf{0} & \mathbf{0} & \mathbf{0} & \mathbf{0} \\ \mathbf{0} & \mathbf{0} & \mathbf{0} & \mathbf{0} \end{bmatrix}, \qquad \mathbf{Q}_{11}^{1} = \begin{bmatrix} \mathbf{0} & \left(\mathbf{N}_{,1}^{e}\right)^{\mathrm{T}}\mathbf{N}_{,1}^{e} & \mathbf{0} & \mathbf{0} \\ \left(\mathbf{N}_{,1}^{e}\right)^{\mathrm{T}}\mathbf{N}_{,1}^{e} & \mathbf{0} & \mathbf{0} & \mathbf{0} \\ \mathbf{0} & \mathbf{0} & \mathbf{0} & \mathbf{0} \\ \mathbf{0} & \mathbf{0} & \mathbf{0} & \mathbf{0} \end{bmatrix},$$

$$\mathbf{Q}_{11}^{2} = \begin{bmatrix} \mathbf{0} & \mathbf{0} & \left(\mathbf{N}_{,1}^{e}\right)^{\mathrm{T}}\mathbf{N}_{,1}^{e} & \mathbf{0} \\ \mathbf{0} & \mathbf{0} & \mathbf{0} & \mathbf{0} \\ \left(\mathbf{N}_{,1}^{e}\right)^{\mathrm{T}}\mathbf{N}_{,1}^{e} & \mathbf{0} & \mathbf{0} & \mathbf{0} \\ \mathbf{0} & \mathbf{0} & \mathbf{0} & \mathbf{0} \end{bmatrix}, \quad \mathbf{Q}_{11}^{3} = \begin{bmatrix} \mathbf{0} & \mathbf{0} & \mathbf{0} & \left(\mathbf{N}_{,1}^{e}\right)^{\mathrm{T}}\mathbf{N}_{,1}^{e} \\ \mathbf{0} & \mathbf{0} & \left(\mathbf{N}_{,1}^{e}\right)^{\mathrm{T}}\mathbf{N}_{,1}^{e} & \mathbf{0} \\ \mathbf{0} & \left(\mathbf{N}_{,1}^{e}\right)^{\mathrm{T}}\mathbf{N}_{,1}^{e} & \mathbf{0} & \mathbf{0} \\ \left(\mathbf{N}_{,1}^{e}\right)^{\mathrm{T}}\mathbf{N}_{,1}^{e} & \mathbf{0} & \mathbf{0} & \mathbf{0} \end{bmatrix},$$

the transverse normal strains E_{22} and E_{33}

$$\mathbf{Q}_{22}^{0} = \begin{bmatrix} \mathbf{0} & \mathbf{0} & \mathbf{0} & \mathbf{0} \\ \mathbf{0} & \left(\mathbf{N}^{e}\right)^{\mathrm{T}}\mathbf{N}^{e} & \mathbf{0} & \mathbf{0} \\ \mathbf{0} & \mathbf{0} & \mathbf{0} & \mathbf{0} \\ \mathbf{0} & \mathbf{0} & \mathbf{0} & \mathbf{0} \end{bmatrix}, \quad \mathbf{Q}_{33}^{0} = \begin{bmatrix} \mathbf{0} & \mathbf{0} & \mathbf{0} & \mathbf{0} \\ \mathbf{0} & \mathbf{0} & \mathbf{0} & \mathbf{0} \\ \mathbf{0} & \mathbf{0} & \left(\mathbf{N}^{e}\right)^{\mathrm{T}}\mathbf{N}^{e} & \mathbf{0} \\ \mathbf{0} & \mathbf{0} & \mathbf{0} & \mathbf{0} \end{bmatrix},$$

and the shear strains E_{12}, E_{13}, and E_{23}

$$\mathbf{Q}_{12}^{0} = \begin{bmatrix} \mathbf{0} & \left(\mathbf{N}_{,1}^{e}\right)^{\mathrm{T}}\mathbf{N}^{e} & \mathbf{0} & \mathbf{0} \\ \left(\mathbf{N}^{e}\right)^{\mathrm{T}}\mathbf{N}_{,1}^{e} & \mathbf{0} & \mathbf{0} & \mathbf{0} \\ \mathbf{0} & \mathbf{0} & \mathbf{0} & \mathbf{0} \\ \mathbf{0} & \mathbf{0} & \mathbf{0} & \mathbf{0} \end{bmatrix}, \qquad \mathbf{Q}_{12}^{1} = \begin{bmatrix} \mathbf{0} & \mathbf{0} & \mathbf{0} & \mathbf{0} \\ \mathbf{0} & \left(\mathbf{N}_{,1}^{e}\right)^{\mathrm{T}}\mathbf{N}^{e} + \left(\mathbf{N}^{e}\right)^{\mathrm{T}}\mathbf{N}_{,1}^{e} & \mathbf{0} & \mathbf{0} \\ \mathbf{0} & \mathbf{0} & \mathbf{0} & \mathbf{0} \\ \mathbf{0} & \mathbf{0} & \mathbf{0} & \mathbf{0} \end{bmatrix},$$

$$\mathbf{Q}_{12}^{2} = \begin{bmatrix} \mathbf{0} & \mathbf{0} & \mathbf{0} & \left(\mathbf{N}_{,1}^{e}\right)^{\mathrm{T}}\mathbf{N}^{e} \\ \mathbf{0} & \mathbf{0} & \left(\mathbf{N}^{e}\right)^{\mathrm{T}}\mathbf{N}_{,1}^{e} & \mathbf{0} \\ \mathbf{0} & \left(\mathbf{N}_{,1}^{e}\right)^{\mathrm{T}}\mathbf{N}^{e} & \mathbf{0} & \mathbf{0} \\ \left(\mathbf{N}^{e}\right)^{\mathrm{T}}\mathbf{N}_{,1}^{e} & \mathbf{0} & \mathbf{0} & \mathbf{0} \end{bmatrix}, \quad \mathbf{Q}_{12}^{3} = \begin{bmatrix} \mathbf{0} & \mathbf{0} & \mathbf{0} & \mathbf{0} \\ \mathbf{0} & \mathbf{0} & \mathbf{0} & \left(\mathbf{N}_{,1}^{e}\right)^{\mathrm{T}}\mathbf{N}^{e} + \left(\mathbf{N}^{e}\right)^{\mathrm{T}}\mathbf{N}_{,1}^{e} \\ \mathbf{0} & \mathbf{0} & \mathbf{0} & \mathbf{0} \\ \mathbf{0} & \left(\mathbf{N}_{,1}^{e}\right)^{\mathrm{T}}\mathbf{N}^{e} + \left(\mathbf{N}^{e}\right)^{\mathrm{T}}\mathbf{N}_{,1}^{e} & \mathbf{0} & \mathbf{0} \end{bmatrix},$$

$$\mathbf{Q}_{13}^{0} = \begin{bmatrix} \mathbf{0} & \mathbf{0} & \left(\mathbf{N}_{,1}^{e}\right)^{\mathrm{T}}\mathbf{N}^{e} & \mathbf{0} \\ \mathbf{0} & \mathbf{0} & \mathbf{0} & \mathbf{0} \\ \left(\mathbf{N}^{e}\right)^{\mathrm{T}}\mathbf{N}_{,1}^{e} & \mathbf{0} & \mathbf{0} & \mathbf{0} \\ \mathbf{0} & \mathbf{0} & \mathbf{0} & \mathbf{0} \end{bmatrix}, \qquad \mathbf{Q}_{13}^{1} = \begin{bmatrix} \mathbf{0} & \mathbf{0} & \mathbf{0} & \left(\mathbf{N}_{,1}^{e}\right)^{\mathrm{T}}\mathbf{N}^{e} \\ \mathbf{0} & \mathbf{0} & \left(\mathbf{N}_{,1}^{e}\right)^{\mathrm{T}}\mathbf{N}^{e} & \mathbf{0} \\ \mathbf{0} & \left(\mathbf{N}^{e}\right)^{\mathrm{T}}\mathbf{N}_{,1}^{e} & \mathbf{0} & \mathbf{0} \\ \left(\mathbf{N}^{e}\right)^{\mathrm{T}}\mathbf{N}_{,1}^{e} & \mathbf{0} & \mathbf{0} & \mathbf{0} \end{bmatrix},$$

$$\mathbf{Q}_{13}^{2} = \begin{bmatrix} \mathbf{0} & \mathbf{0} & \mathbf{0} & \mathbf{0} \\ \mathbf{0} & \mathbf{0} & \mathbf{0} & \mathbf{0} \\ \mathbf{0} & \mathbf{0} & \left(\mathbf{N}_{,1}^{e}\right)^{\mathrm{T}}\mathbf{N}^{e} + \left(\mathbf{N}^{e}\right)^{\mathrm{T}}\mathbf{N}_{,1}^{e} & \mathbf{0} \\ \mathbf{0} & \mathbf{0} & \mathbf{0} & \mathbf{0} \end{bmatrix}, \qquad \mathbf{Q}_{13}^{3} = \begin{bmatrix} \mathbf{0} & \mathbf{0} & \mathbf{0} & \mathbf{0} \\ \mathbf{0} & \mathbf{0} & \mathbf{0} & \mathbf{0} \\ \mathbf{0} & \mathbf{0} & \mathbf{0} & \left(\mathbf{N}_{,1}^{e}\right)^{\mathrm{T}}\mathbf{N}^{e} + \left(\mathbf{N}^{e}\right)^{\mathrm{T}}\mathbf{N}_{,1}^{e} \\ \mathbf{0} & \mathbf{0} & \left(\mathbf{N}_{,1}^{e}\right)^{\mathrm{T}}\mathbf{N}^{e} + \left(\mathbf{N}^{e}\right)^{\mathrm{T}}\mathbf{N}_{,1}^{e} & \mathbf{0} \end{bmatrix},$$

$$\mathbf{Q}_{23}^{0} = \begin{bmatrix} \mathbf{0} & \mathbf{0} & \mathbf{0} & \mathbf{0} \\ \mathbf{0} & \mathbf{0} & \left(\mathbf{N}^{e}\right)^{\mathrm{T}}\mathbf{N}^{e} & \mathbf{0} \\ \mathbf{0} & \left(\mathbf{N}^{e}\right)^{\mathrm{T}}\mathbf{N}^{e} & \mathbf{0} & \mathbf{0} \\ \mathbf{0} & \mathbf{0} & \mathbf{0} & \mathbf{0} \end{bmatrix}, \qquad \mathbf{Q}_{23}^{1} = \begin{bmatrix} \mathbf{0} & \mathbf{0} & \mathbf{0} & \mathbf{0} \\ \mathbf{0} & \mathbf{0} & \mathbf{0} & \left(\mathbf{N}^{e}\right)^{\mathrm{T}}\mathbf{N}^{e} \\ \mathbf{0} & \mathbf{0} & \mathbf{0} & \mathbf{0} \\ \mathbf{0} & \left(\mathbf{N}^{e}\right)^{\mathrm{T}}\mathbf{N}^{e} & \mathbf{0} & \mathbf{0} \end{bmatrix},$$

$$\mathbf{Q}_{23}^{2} = \begin{bmatrix} \mathbf{0} & \mathbf{0} & \mathbf{0} & \mathbf{0} \\ \mathbf{0} & \mathbf{0} & \mathbf{0} & \mathbf{0} \\ \mathbf{0} & \mathbf{0} & \mathbf{0} & \left(\mathbf{N}^{e}\right)^{\mathrm{T}}\mathbf{N}^{e} \\ \mathbf{0} & \mathbf{0} & \left(\mathbf{N}^{e}\right)^{\mathrm{T}}\mathbf{N}^{e} & \mathbf{0} \end{bmatrix}, \qquad \mathbf{Q}_{23}^{3} = \begin{bmatrix} \mathbf{0} & \mathbf{0} & \mathbf{0} & \mathbf{0} \\ \mathbf{0} & \mathbf{0} & \mathbf{0} & \mathbf{0} \\ \mathbf{0} & \mathbf{0} & \mathbf{0} & \mathbf{0} \\ \mathbf{0} & \mathbf{0} & \mathbf{0} & \left(\mathbf{N}^{e}\right)^{\mathrm{T}}\mathbf{N}^{e} + \left(\mathbf{N}^{e}\right)^{\mathrm{T}}\mathbf{N}^{e} \end{bmatrix},$$

such that the element matrices $\mathbf{N}^{e}$ and $\mathbf{N}_{,1}^{e}$ collect the shape functions and their derivatives with respect ξ^{1}, respectively. We highlight that the adopted kinematics of the solid-beam model, which follows a 1-dimensional interpolation of both the geometry and the displacement field (see Section 2), allows for a flexible description of the problem and, at the same time, strongly simplifies the input and the operator construction at the element level, thereby improving the efficiency of the nonlinear solver.

Appendix C. Integration of the generalized constitutive law along the cross-section coordinate directions

In this appendix, we provide a flowchart that illustrates the intermediate steps to analytically evaluate the generalized constitutive matrix (42).

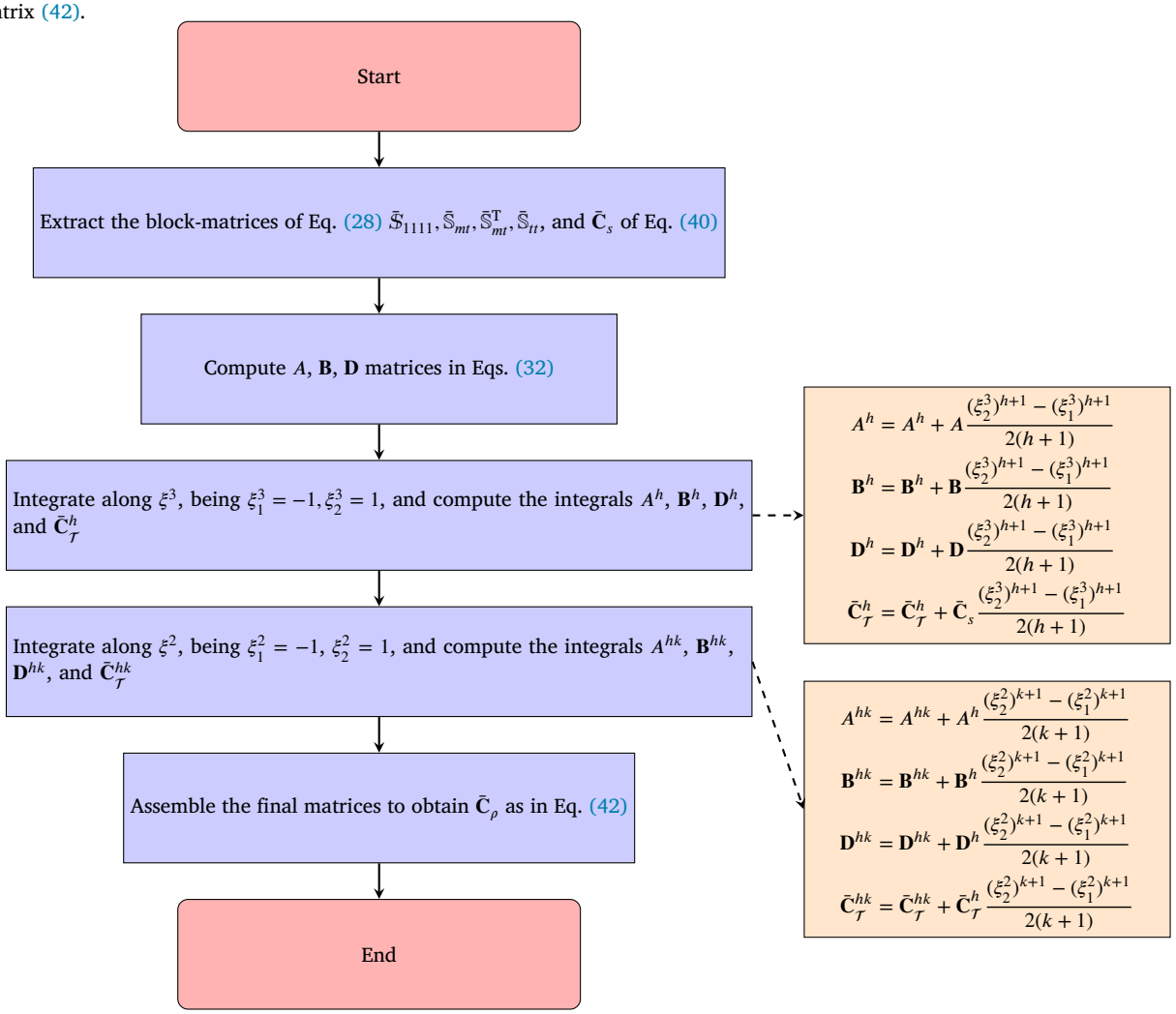

We remark that the extension of the outlined process to layered structures is straightforward.

Data availability

The data that support the fundings of this study are available from the authors upon reasonable request.

References

[1] D. Hodges, Nonlinear Composite Beam Theory, American Institute of Aeronautics and Astronautics, Reston, Virginia, 2006.
[2] L. Leonetti, F. Liguori, D. Magisano, G. Garcea, An efficient isogeometric solid-shell formulation for geometrically nonlinear analysis of elastic shells, Comput. Methods Appl. Mech. Engrg. 331 (2018) 159–183, http://dx.doi.org/10.1016/j.cma.2017.11.025, URL http://www.sciencedirect.com/science/article/pii/S0045782517307429.
[3] A. Sabale, K.N. Gopal, Nonlinear aeroelastic response of wind turbines using Simo-Vu-Quoc rods, Appl. Math. Model. 65 (2019) 696–716, http://dx.doi.org/10.1016/j.apm.2018.09.003, URL http://www.sciencedirect.com/science/article/pii/S0307904X18304438.
[4] J. Simo, A three dimensional finite-strain rod model. Part II: Computational aspect, Comput. Methods Appl. Mech. Engrg. 58 (1986) 79–116.
[5] P. Betsch, A. Menzel, E. Stein, On the parametrization of finite rotations in computational mechanics: A classification of concepts with application to smooth shells, Comput. Methods Appl. Mech. Engrg. 155 (3) (1998) 273–305, http://dx.doi.org/10.1016/S0045-7825(97)00158-8, URL http://www.sciencedirect.com/science/article/pii/S0045782597001588.
[6] A. Ibrahimbegovic, R.L. Taylor, On the role of frame-invariance in structural mechanics models at finite rotations, Comput. Methods Appl. Mech. Engrg. 191 (45) (2002) 5159–5176, http://dx.doi.org/10.1016/S0045-7825(02)00442-5, URL http://www.sciencedirect.com/science/article/pii/S0045782502004425.
[7] J. Simo, A finite strain beam formulation. The three-dimensional dynamic problem. Part I, Comput. Methods Appl. Mech. Engrg. 49 (1) (1985) 55–70, http://dx.doi.org/10.1016/0045-7825(85)90050-7, URL http://www.sciencedirect.com/science/article/pii/0045782585900507.

[8] A. Cardona, M. Geradin, A beam finite element non-linear theory with finite rotations, Internat. J. Numer. Methods Engrg. 26 (11) (1988) 2403–2438, http://dx.doi.org/10.1002/nme.1620261105, URL https://onlinelibrary.wiley.com/doi/abs/10.1002/nme.1620261105, arXiv:https://onlinelibrary.wiley.com/doi/pdf/10.1002/nme.1620261105.
[9] D. Zupan, M. Saje, The three-dimensional beam theory: Finite element formulation based on curvature, Comput. Struct. 81 (18) (2003) 1875–1888, http://dx.doi.org/10.1016/S0045-7949(03)00208-6, Civil Comp Special Issue. URL http://www.sciencedirect.com/science/article/pii/S0045794903002086.
[10] S. Lopez, Three-dimensional finite rotations treatment based on a minimal set parameterization and vector space operations in beam elements, Comput. Mech. 52 (2) (2013) 377–399, http://dx.doi.org/10.1007/s00466-012-0818-3.
[11] B. Oesterle, R. Sachse, E. Ramm, M. Bischoff, Hierarchic isogeometric large rotation shell elements including linearized transverse shear parametrization, Comput. Methods Appl. Mech. Engrg. 321 (2017) 383–405, http://dx.doi.org/10.1016/j.cma.2017.03.031, URL http://www.sciencedirect.com/science/article/pii/S0045782517302323.
[12] F.S. Liguori, A. Madeo, D. Magisano, L. Leonetti, G. Garcea, Post-buckling optimisation strategy of imperfection sensitive composite shells using koiter method and Monte Carlo simulation, Compos. Struct. 192 (2018) 654–670, http://dx.doi.org/10.1016/j.compstruct.2018.03.023, URL http://www.sciencedirect.com/science/article/pii/S0263822317339776.
[13] F.S. Liguori, G. Zucco, A. Madeo, D. Magisano, L. Leonetti, G. Garcea, P.M. Weaver, Postbuckling optimisation of a variable angle tow composite wingbox using a multi-modal Koiter approach, Thin-Walled Struct. 138 (2019) 183–198, http://dx.doi.org/10.1016/j.tws.2019.01.035, URL http://www.sciencedirect.com/science/article/pii/S0263823118316331.
[14] D. Magisano, L. Leonetti, G. Garcea, Isogeometric analysis of 3D beams for arbitrarily large rotations: Locking-free and path-independent solution without displacement DOFs inside the patch, Comput. Methods Appl. Mech. Engrg. 373 (2021) 113437, http://dx.doi.org/10.1016/j.cma.2020.113437, URL https://www.sciencedirect.com/science/article/pii/S0045782520306228.
[15] E. Reissner, On finite deformations of space-curved beams, Z. Angew. Math. Phys. ZAMP 32 (6) (1981) 734–744, http://dx.doi.org/10.1007/BF00946983.
[16] A. Ibrahimbegovic, On the choice of finite rotation parameters, Comput. Methods Appl. Mech. Engrg. 149 (1) (1997) 49–71, http://dx.doi.org/10.1016/S0045-7825(97)00059-5, Containing papers presented at the Symposium on Advances in Computational Mechanics. URL http://www.sciencedirect.com/science/article/pii/S0045782597000595.
[17] M. Ritto-Correa, D. Camotim, On the differentiation of the Rodrigues formula and its significance for the vector-like parameterization of Reissner-Simo beam theory, Internat. J. Numer. Methods Engrg. 55 (9) (2002) 1005–1032, http://dx.doi.org/10.1002/nme.532, URL https://onlinelibrary.wiley.com/doi/abs/10.1002/nme.532, arXiv:https://onlinelibrary.wiley.com/doi/pdf/10.1002/nme.532.
[18] R. Goncalves, M. Ritto-Correa, D. Camotim, A large displacement and finite rotation thin-walled beam formulation including cross-section deformation, Comput. Methods Appl. Mech. Engrg. 199 (23) (2010) 1627–1643, http://dx.doi.org/10.1016/j.cma.2010.01.006, URL http://www.sciencedirect.com/science/article/pii/S0045782510000150.
[19] E. Marino, Locking-free isogeometric collocation formulation for three-dimensional geometrically exact shear-deformable beams with arbitrary initial curvature, Comput. Methods Appl. Mech. Engrg. 324 (2017) 546–572, http://dx.doi.org/10.1016/j.cma.2017.06.031, URL http://www.sciencedirect.com/science/article/pii/S0045782517305455.
[20] E. Marino, J. Kiendl, L.D. Lorenzis, Explicit isogeometric collocation for the dynamics of three-dimensional beams undergoing finite motions, Comput. Methods Appl. Mech. Engrg. 343 (2019) 530–549, http://dx.doi.org/10.1016/j.cma.2018.09.005, URL http://www.sciencedirect.com/science/article/pii/S0045782518304481.
[21] E. Marino, J. Kiendl, L. De Lorenzis, Isogeometric collocation for implicit dynamics of three-dimensional beams undergoing finite motions, Comput. Methods Appl. Mech. Engrg. 356 (2019) 548–570, http://dx.doi.org/10.1016/j.cma.2019.07.013, URL http://www.sciencedirect.com/science/article/pii/S0045782519304098.
[22] M. Crisfield, G. Moita, A unified co-rotational framework for solids, shells and beams, Int. J. Solids Struct. 33 (20) (1996) 2969–2992, http://dx.doi.org/10.1016/0020-7683(95)00252-9, URL http://www.sciencedirect.com/science/article/pii/0020768395002529.
[23] R. Alsafadie, M. Hjiaj, J.-M. Battini, Corotational mixed finite element formulation for thin-walled beams with generic cross-section, Comput. Methods Appl. Mech. Engrg. 199 (49) (2010) 3197–3212, http://dx.doi.org/10.1016/j.cma.2010.06.026, URL http://www.sciencedirect.com/science/article/pii/S0045782510001933.
[24] S. de Miranda, A. Madeo, D. Melchionda, L. Patruno, A. Ruggerini, A corotational based geometrically nonlinear generalized beam theory: buckling FE analysis, Int. J. Solids Struct. 121 (2017) 212–227, http://dx.doi.org/10.1016/j.ijsolstr.2017.05.030, URL http://www.sciencedirect.com/science/article/pii/S002076831730241X.
[25] C.C. Rankin, F.A. Brogan, An element independent corotational procedure for the treatment of large rotations, J. Press. Vessel. Technol. 108 (2) (1986) 165–174, http://dx.doi.org/10.1115/1.3264765, arXiv:https://asmedigitalcollection.asme.org/pressurevesseltech/article-pdf/108/2/165/5534963/165_1.pdf.
[26] G. Garcea, A. Madeo, R. Casciaro, Nonlinear FEM analysis for beams and plate assemblages based on the implicit corotational method, J. Mech. Mater. Struct. 7 (6) (2012) 539–574, http://dx.doi.org/10.2140/jomms.2012.7.539.
[27] G. Garcea, A. Madeo, R. Casciaro, The implicit corotational method and its use in the derivation of nonlinear structural models for beams and plates, J. Mech. Mater. Struct. 7 (6) (2012) 509–539, http://dx.doi.org/10.2140/jomms.2012.7.509.
[28] G. Jelenić, M. Crisfield, Geometrically exact 3D beam theory: implementation of a strain - invariant finite element for statics and dynamics, Comput. Methods Appl. Mech. Engrg. 171 (1) (1999) 141–171, http://dx.doi.org/10.1016/S0045-7825(98)00249-7, URL http://www.sciencedirect.com/science/article/pii/S0045782598002497.
[29] D. Magisano, L. Leonetti, A. Madeo, G. Garcea, A large rotation finite element analysis of 3D beams by incremental rotation vector and exact strain measure with all the desirable features, Comput. Methods Appl. Mech. Engrg. 361 (2020) 112811, http://dx.doi.org/10.1016/j.cma.2019.112811, URL http://www.sciencedirect.com/science/article/pii/S0045782519307030.
[30] A.G. Holzapfel, Nonlinear Solid Mechanics, John Wiley Sons, New-York, 2000.
[31] S. Reese, P. Wriggers, B. Reddy, New locking-free brick element technique for large deformation problems in elasticity, Comput. Struct. 75 (3) (2000) 291–304, http://dx.doi.org/10.1016/S0045-7949(99)00137-6.
[32] K. Sze, W. Chan, T. Pian, An eight-node hybrid-stress solid-shell element for geometric non-linear analysis of elastic shells, Internat. J. Numer. Methods Engrg. 55 (7) (2002) 853–878, http://dx.doi.org/10.1002/nme.535, URL https://onlinelibrary.wiley.com/doi/abs/10.1002/nme.535.
[33] D. Magisano, L. Leonetti, G. Garcea, Advantages of the mixed format in geometrically nonlinear analysis of beams and shells using solid finite elements, Internat. J. Numer. Methods Engrg. 109 (9) (2017) 1237–1262, http://dx.doi.org/10.1002/nme.5322, URL https://onlinelibrary.wiley.com/doi/abs/10.1002/nme.5322, arXiv:https://onlinelibrary.wiley.com/doi/pdf/10.1002/nme.5322.
[34] D. Magisano, L. Leonetti, G. Garcea, How to improve efficiency and robustness of the Newton method in geometrically non-linear structural problem discretized via displacement-based finite elements, Comput. Methods Appl. Mech. Engrg. 313 (2017) 986–1005, http://dx.doi.org/10.1016/j.cma.2016.10.023.
[35] L. Leonetti, D. Magisano, F. Liguori, G. Garcea, An isogeometric formulation of the Koiter's theory for buckling and initial post-buckling analysis of composite shells, Comput. Methods Appl. Mech. Engrg. 337 (2018) 387–410, http://dx.doi.org/10.1016/j.cma.2018.03.037, URL http://www.sciencedirect.com/science/article/pii/S0045782518301610.
[36] J. Frischkorn, S. Reese, A solid-beam finite element and non-linear constitutive modelling, Comput. Methods Appl. Mech. Engrg. 265 (2013) 195–212, http://dx.doi.org/10.1016/j.cma.2013.06.009, URL https://www.sciencedirect.com/science/article/pii/S0045782513001618.

[37] G. Wei, P. Lardeur, F. Druesne, Free vibration analysis of thin to thick straight or curved beams by a solid-3D beam finite element method, Thin-Walled Struct. 191 (2023) 111028, http://dx.doi.org/10.1016/j.tws.2023.111028, URL https://www.sciencedirect.com/science/article/pii/S0263823123005062.
[38] A. Shafqat, O. Weeger, B.-X. Xu, A robust finite strain isogeometric solid-beam element, Comput. Methods Appl. Mech. Engrg. 426 (2024) 116993, http://dx.doi.org/10.1016/j.cma.2024.116993, URL https://www.sciencedirect.com/science/article/pii/S0045782524002494.
[39] M. Bischoff, E. Ramm, Shear deformable shell elements for large strains and rotations, Internat. J. Numer. Methods Engrg. 40 (23) (1997) 4427–4449, http://dx.doi.org/10.1002/(SICI)1097-0207(19971215)40:23<4427::AID-NME268>3.0.CO;2-9, URL https://onlinelibrary.wiley.com/doi/abs/10.1002.
[40] X. Tan, L. Vu-Quoc, Efficient and accurate multilayer solid-shell element: non-linear materials at finite strain, Internat. J. Numer. Methods Engrg. 63 (15) (2005) 2124–2170, http://dx.doi.org/10.1002/nme.1360.
[41] J. Simo, M. Rifai, A class of mixed assumed strain methods and the method of incompatible modes, Internat. J. Numer. Methods Engrg. 29 (8) (1990) 1595–1638, http://dx.doi.org/10.1002/nme.1620290802.
[42] J. Simo, F. Armero, Geometrically non-linear enhanced strain mixed methods and the method of incompatible modes, Internat. J. Numer. Methods Engrg. 33 (7) (1992) 1413–1449, http://dx.doi.org/10.1002/nme.1620330705, URL https://onlinelibrary.wiley.com/doi/abs/10.1002/nme.1620330705, arXiv:https://onlinelibrary.wiley.com/doi/pdf/10.1002/nme.1620330705.
[43] S. Reese, A large deformation solid-shell concept based on reduced integration with hourglass stabilization, Internat. J. Numer. Methods Engrg. 69 (8) (2007) 1671–1716, http://dx.doi.org/10.1002/nme.1827.
[44] D.S. Malkus, T.J. Hughes, Mixed finite element methods - Reduced and selective integration techniques: A unification of concepts, Comput. Methods Appl. Mech. Engrg. 15 (1) (1978) 63–81, http://dx.doi.org/10.1016/0045-7825(78)90005-1, URL https://www.sciencedirect.com/science/article/pii/0045782578900051.
[45] R.P. Cardoso, J.W. Yoon, M. Mahardika, S. Choudhry, R. Alves de Sousa, R. Fontes Valente, Enhanced assumed strain (EAS) and assumed natural strain (ANS) methods for one-point quadrature solid-shell elements, Internat. J. Numer. Methods Engrg. 75 (2) (2008) 156–187, http://dx.doi.org/10.1002/nme.2250.
[46] M. Schwarze, S. Reese, A reduced integration solid-shell finite element based on EAS and the ANS concept: Large deformation problems, Internat. J. Numer. Methods Engrg. (85) (2011) 289–329, http://dx.doi.org/10.1002/nme.
[47] Q. Li, Y. Liu, Z. Zhang, W. Zhong, A new reduced integration solid-shell element based on EAS and ANS with hourglass stabilization, Internat. J. Numer. Methods Engrg. (2015) 1885–1891, http://dx.doi.org/10.1002/nme, arXiv:1010.1724.
[48] T.H. Pian, C.-C. Wu, Hybrid and Incompatible Finite Element Methods, Chapman & All, CRC, New-York, 1969.
[49] K. Sze, A. Ghali, Hybrid hexahedral element for solids, plates, shells and beams by selective scaling, Internat. J. Numer. Methods Engrg. 36 (9) (1993) 1519–1540.
[50] L. Vu-Quoc, X. Tan, Efficient Hybrid-EAS solid element for accurate stress prediction in thick laminated beams, plates, and shells, Comput. Methods Appl. Mech. Engrg. 253 (2013) 337–355, http://dx.doi.org/10.1016/j.cma.2012.07.025.
[51] S. Klinkel, F. Gruttmann, W. Wagner, A robust non-linear solid shell element based on a mixed variational formulation, Comput. Methods Appl. Mech. Engrg. 195 (1–3) (2006) 179–201, http://dx.doi.org/10.1016/j.cma.2005.01.013.
[52] G. Garcea, G. Trunfio, R. Casciaro, Mixed formulation and locking in path-following nonlinear analysis, Comput. Methods Appl. Mech. Engrg. 165 (1–4) (1998) 247–272.
[53] G. Garcea, Mixed formulation in koiter analysis of thin-walled beams, Comput. Methods Appl. Mech. Engrg. 190 (26–27) (2001) 3369–3399.
[54] T. Hughes, J. Cottrell, Y. Bazilevs, Isogeometric analysis: CAD, finite elements, NURBS, exact geometry and mesh refinement, Comput. Methods Appl. Mech. Engrg. 194 (2005) 4135–4195, http://dx.doi.org/10.1016/j.cma.2004.10.008.
[55] G. Marchiori, A. Neto, Isogeometric analysis applied to 2D Bernoulli-Euler beam model: imposition of constraints by Lagrange and Penalty methods, Lat. Am. J. Solids Struct. 17 (2020) http://dx.doi.org/10.1590/1679-78255578.
[56] A. Borković, B. Marussig, G. Radenković, Geometrically exact static isogeometric analysis of arbitrarily curved plane Bernoulli–Euler beam, Thin-Walled Struct. 170 (2022) 108539, http://dx.doi.org/10.1016/j.tws.2021.108539.
[57] A. Patton, S. Faroughi, A. Reali, Efficient equilibrium-based stress recovery for isogeometric laminated Euler–Bernoulli curved beams, Compos. Struct. 345 (2024) 118374, http://dx.doi.org/10.1016/j.compstruct.2024.118374.
[58] R. Bouclier, T. Elguedj, A. Combescure, Locking free isogeometric formulations of curved thick beams, Comput. Methods Appl. Mech. Engrg. 245–246 (2012) 144–162, http://dx.doi.org/10.1016/j.cma.2012.06.008.
[59] J. Kiendl, F. Auricchio, T. Hughes, A. Reali, Single-variable formulations and isogeometric discretizations for shear deformable beams, Comput. Methods Appl. Mech. Engrg. 284 (2015) 988–1004, http://dx.doi.org/10.1016/j.cma.2014.11.011, Isogeometric Analysis Special Issue.
[60] L. Greco, M. Cuomo, An implicit G1 multi patch B-spline interpolation for Kirchhoff–Love space rod, Comput. Methods Appl. Mech. Engrg. 269 (2014) 173–197, http://dx.doi.org/10.1016/j.cma.2013.09.018.
[61] D. Benson, Y. Bazilevs, M. Hsu, T. Hughes, Isogeometric shell analysis: The Reissner–Mindlin shell, Comput. Methods Appl. Mech. Engrg. 199 (2010) 276–289, http://dx.doi.org/10.1016/j.cma.2009.05.011, Computational Geometry and Analysis.
[62] W. Dornisch, S. Klinkel, B. Simeon, Isogeometric Reissner–Mindlin shell analysis with exactly calculated director vectors, Comput. Methods Appl. Mech. Engrg. 253 (2013) 491–504, http://dx.doi.org/10.1016/j.cma.2012.09.010.
[63] J. Kiendl, K.-U. Bletzinger, J. Linhard, R. Wüchner, Isogeometric shell analysis with Kirchhoff–Love elements, Comput. Methods Appl. Mech. Engrg. 198 (2009) 3902–3914, http://dx.doi.org/10.1016/j.cma.2009.08.013.
[64] J. Kiendl, M.-C. Hsu, M.C. Wu, A. Reali, Isogeometric Kirchhoff–Love shell formulations for general hyperelastic materials, Comput. Methods Appl. Mech. Engrg. 291 (2015) 280–303, http://dx.doi.org/10.1016/j.cma.2015.03.010.
[65] H. Casquero, L. Liu, Y. Zhang, A. Reali, J. Kiendl, H. Gomez, Arbitrary-degree T-splines for isogeometric analysis of fully nonlinear Kirchhoff–Love shells, Comput.-Aided Des. 82 (2017) 140–153, http://dx.doi.org/10.1016/j.cad.2016.08.009.
[66] L. Leonetti, D. Magisano, A. Madeo, G. Garcea, J. Kiendl, A. Reali, A simplified Kirchhoff-Love large deformation model for elastic shells and its effective isogeometric formulation, Comput. Methods Appl. Mech. Engrg. 354 (2019) 369–396, http://dx.doi.org/10.1016/j.cma.2019.05.025, URL http://www.sciencedirect.com/science/article/pii/S0045782519302956.
[67] L. Coradello, D. D'Angella, M. Carraturo, J. Kiendl, S. Kollmannsberger, E. R., A. Reali, Hierarchically refined isogeometric analysis of trimmed shells, Comput. Mech. 66 (2020) 431–447, http://dx.doi.org/10.1007/s00466-020-01858-6.
[68] J. Caseiro, R. Valente, A. Reali, J. Kiendl, F. Auricchio, R.A. de Sousa, Assumed Natural Strain NURBS-based solid-shell element for the analysis of large deformation elasto-plastic thin-shell structures, Comput. Methods Appl. Mech. Engrg. 284 (2015) 861–880, http://dx.doi.org/10.1016/j.cma.2014.10.037, Isogeometric Analysis Special Issue. URL http://www.sciencedirect.com/science/article/pii/S0045782514004071.
[69] R. Bouclier, T. Elguedj, A. Combescure, Efficient isogeometric NURBS-based solid-shell elements: Mixed formulation and B-method, Comput. Methods Appl. Mech. Engrg. 267 (2013) 86–110, http://dx.doi.org/10.1016/j.cma.2013.08.002.
[70] R. Bouclier, T. Elguedj, A. Combescure, An isogeometric locking-free NURBS-based solid-shell element for geometrically nonlinear analysis, Internat. J. Numer. Methods Engrg. 101 (10) (2015) 774–808, http://dx.doi.org/10.1002/nme.4834.
[71] H. Casquero, K.D. Mathews, Overcoming membrane locking in quadratic NURBS-based discretizations of linear Kirchhoff-Love shells: CAS elements, Comput. Methods Appl. Mech. Engrg. 417 (2023) 116523, http://dx.doi.org/10.1016/j.cma.2023.116523, URL https://www.sciencedirect.com/science/article/pii/S0045782523006473.

[72] T.M. Le, H. Nguyen-Xuan, L. Leonetti, A new paradigm coupling element-wise discrete-strain gaps with patch-wise reduced integration for efficient isogeometric nonlinear Kirchhoff–Love shell analysis, Comput. Methods Appl. Mech. Engrg. 436 (2025) 117667, http://dx.doi.org/10.1016/j.cma.2024.117667, URL https://www.sciencedirect.com/science/article/pii/S0045782524009216.

[73] L. Leonetti, J. Kiendl, A mixed integration point (MIP) formulation for hyperelastic Kirchhoff - Love shells for nonlinear static and dynamic analysis, Comput. Methods Appl. Mech. Engrg. 416 (2023) 116325, http://dx.doi.org/10.1016/j.cma.2023.116325, URL https://www.sciencedirect.com/science/article/pii/S0045782523004498.

[74] C. Adam, T. Hughes, S. Bouabdallah, M. Zarroug, H. Maitournam, Selective and reduced numerical integrations for NURBS-based isogeometric analysis, Comput. Methods Appl. Mech. Engrg. 284 (2015) 732–761, http://dx.doi.org/10.1016/j.cma.2014.11.001.

[75] D. Magisano, L. Leonetti, G. Garcea, How to improve efficiency and robustness of the Newton method in geometrically non-linear structural problem discretized via displacement-based finite elements, Comput. Methods Appl. Mech. Engrg. 313 (2017) 986–1005.

[76] L. Leonardo, V.H. M., A hierarchic isogeometric hyperelastic solid-shell, Comput. Mech. (2024) http://dx.doi.org/10.1007/s00466-024-02452-w.

[77] T.X. Duong, L. Leonetti, J. Kiendl, A variationally consistent contact formulation based on a mixed interpolation point method and isogeometric discretization, Comput. Methods Appl. Mech. Engrg. 417 (2023) 116361, http://dx.doi.org/10.1016/j.cma.2023.116361, A Special Issue in Honor of the Lifetime Achievements of T. J. R. Hughes. URL https://www.sciencedirect.com/science/article/pii/S0045782523004851.

[78] A. Patton, L. Leonetti, J. Kiendl, An isogeometric assumed natural strain method to alleviate locking in solid beams, Comput. Methods Appl. Mech. Engrg. 442 (2025) 118024, http://dx.doi.org/10.1016/j.cma.2025.118024, URL https://www.sciencedirect.com/science/article/pii/S0045782525002968.

[79] Z.-H. Guo, M. Chi-Sing, Conjugate stress and tensor equation $\sum_{r=1}^{m} \mathbf{U}^{m-1}\mathbf{X}\mathbf{U}^{r-1} = \mathbf{C}$, Int. J. Solids Struct. 29 (16) (1992) 2063–2076, http://dx.doi.org/10.1016/0020-7683(92)90194-X.

[80] R. Hauptmann, K. Schweizerhof, A systematic development of 'solid-shell' element formulations for linear and non-linear analyses employing only displacement degrees of freedom, Internat. J. Numer. Methods Engrg. 42 (1) (1998) 49–69, http://dx.doi.org/10.1002/(SICI)1097-0207(19980515)42:1<49::AID-NME349>3.0.CO;2-2.

[81] D. Magisano, L. Leonetti, G. Garcea, Koiter asymptotic analysis of multilayered composite structures using mixed solid-shell finite elements, Compos. Struct. 154 (2016) 296–308, http://dx.doi.org/10.1016/j.compstruct.2016.07.046.

[82] M. Loibl, L. Leonetti, A. Reali, J. Kiendl, Patch-wise quadrature of trimmed surfaces in Isogeometric Analysis, Comput. Methods Appl. Mech. Engrg. 415 (2023) 116279, http://dx.doi.org/10.1016/j.cma.2023.116279, URL https://www.sciencedirect.com/science/article/pii/S0045782523004036.

[83] D. Magisano, A. Corrado, New robust and efficient global iterations for large deformation finite element analysis of beams and shells with material nonlinearity, Comput. Methods Appl. Mech. Engrg. 406 (2023) 115900, http://dx.doi.org/10.1016/j.cma.2023.115900, URL https://www.sciencedirect.com/science/article/pii/S0045782523000233.

[84] M.-J. Choi, R.A. Sauer, S. Klinkel, A selectively reduced degree basis for efficient mixed nonlinear isogeometric beam formulations with extensible directors, Comput. Methods Appl. Mech. Engrg. 417 (2023) 116387, http://dx.doi.org/10.1016/j.cma.2023.116387, A Special Issue in Honor of the Lifetime Achievements of T. J. R. Hughes. URL https://www.sciencedirect.com/science/article/pii/S004578252300511X.

[85] E.N. Dvorkin, E. Onte, J. Oliver, On a non-linear formulation for curved Timoshenko beam elements considering large displacement/rotation increments, Internat. J. Numer. Methods Engrg. 26 (7) (1988) 1597–1613, http://dx.doi.org/10.1002/nme.1620260710, URL https://onlinelibrary.wiley.com/doi/abs/10.1002/nme.1620260710.

[86] J. Rhim, S.W. Lee, A vectorial approach to computational modelling of beams undergoing finite rotations, Internat. J. Numer. Methods Engrg. 41 (3) (1998) 527–540, http://dx.doi.org/10.1002/(SICI)1097-0207(19980215)41:3<527::AID-NME297>3.0.CO;2-7.

[87] D. Magisano, L. Leonetti, G. Garcea, Isogeometric analysis of 3D beams for arbitrarily large rotations: Locking-free and path-independent solution without displacement DOFs inside the patch, Comput. Methods Appl. Mech. Engrg. 373 (2021) 113437, http://dx.doi.org/10.1016/j.cma.2020.113437, URL https://www.sciencedirect.com/science/article/pii/S0045782520306228.

[88] C. Cho, H.C. Park, S.W. Lee, Stability analysis using a geometrically nonlinear assumed strain solid shell element model, Finite Elem. Anal. Des. 29 (2) (1998) 121–135, http://dx.doi.org/10.1016/S0168-874X(98)00021-3, URL https://www.sciencedirect.com/science/article/pii/S0168874X98000213.

[89] J. Huddleston, Finite deflections and snap-through of high circular arches, J. Appl. Mech. 35 (4) (1968) 763–769, http://dx.doi.org/10.1115/1.3601302, arXiv:https://asmedigitalcollection.asme.org/appliedmechanics/article-pdf/35/4/763/5449474/763_1.pdf.

[90] Maplesoft, a division of Waterloo Maple Inc., Maple, 2019, URL https://hadoop.apache.org.